Lithos 364–365 (2020) 105510

Contents lists available at ScienceDirect

Lithos

journal homepage: www.elsevier.com/locate/lithos

Research Article

Jurassic segmentation of the early Andean magmatic Province in southern central Chile (35–39°S): Petrological constrains and tectonic drivers

P. Rossel [a,*], A. Echaurren [b], M.N. Ducea [c,d], P. Maldonado [a], K. Llanos [a]

[a] Universidad Andres Bello, Facultad de Ingeniería, Geología, Autopista Talcahuano, 7100 Concepcion, Chile
[b] Universidad de Buenos Aires, Facultad de Ciencias Exactas y Naturales, Instituto de Estudios Andinos, Conicet-Universidad de Buenos Aires, C1428EHA Buenos Aires, Argentina
[c] Department of Geosciences, University of Arizona, Tucson, AZ 85721, USA
[d] Faculty of Geology and Geophysics, University of Bucharest, Bucharest 010041, Romania

ARTICLE INFO

Article history:
Received 10 September 2019
Received in revised form 23 March 2020
Accepted 24 March 2020
Available online 25 March 2020

Keywords:
Early Andes
Jurassic magmatism
Geochronology
Sr-Nd-Pb Isotopes

ABSTRACT

Jurassic volcanismin Southern-Central Chile (35°–39°S) is represented mainly by two units. The first characterized by the volcanic and subvolcanic mostly andesitic deposits of the Altos de Hualmapu Formation, located in actual Coastal Cordillera (35°–35°30′S) and the second corresponding to the lower basaltic and upper andesitic to dacitic upper member of Nacientes del Biobio Formation, in actual Main Cordillera (39°S). Both units mark the transition between northern and patagonian segments of Early Andean Magmatic Province (EAMP) that reach its maximum magmatic activity in this area during late Middle Jurassic in Coastal Cordillera, after two minor pulses of activity between Upper Triassic and Lower Jurassic. No evidence of arc activity is recorded in this area after 155 Ma, when volcanic axis seems to shift to actual Main Cordillera until Lower Cretaceous when it is resumed again to the west. The discontinuity of the arc front suggest the presence of a major cutoff in axis at ≈36–37°. Whole rock geochemical and isotopical Sr-Nd-Pb data shows that this areal discontinuity coincides with an enrichment of the magmas that suggest ≈20–30% of participation of an enriched source in the genesis of the magmas. Given the mostly extensional to transtensional tectonic regime of Western Gondwana during Jurassic and Lower Cretaceous it is unlike to assume high degrees of assimilation at shallow levels, so the observed enrichment should reflect the addition of fertile asthenospheric mantle dragged by the slab as result of the massive roll back and tearing of the oceanic plate under the Arc in Patagonia during Upper Triassic and Middle Jurassic.

1. Introduction

For a length of over ~4000 km, the Chilean margin of western South America represents a long-lived subduction zone where arc magmatism and orogenic processes have developed since Paleozoic time. They were driven by the eastward subduction of Panthalassic/Pacific plates beneath the Gondwana/South American continent (Mpodozis and Ramos, 1989). In this ocean-continent convergent setting, the magmatic arc is formed by a partial melting of the mantle wedge, fed by fluids coming from the dehydration of subducted oceanic lithosphere (Grove et al., 2002). Building of a continuous arc and magmatic addition to the upper plate takes place episodically (Paterson and Ducea, 2015), and develops parallel-to-the-trench (e.g., Stern, 2002).

Along this subduction zone (~18–54°S), magmatic arcs of different ages are exposed as batholiths and volcanic-volcanoclastic units that form the bulk of the middle-upper continental crust (e.g., Mpodozis and Ramos, 1989). They are located at variable distances from the present trench and they constitute different portions of the present morphostructural units of the margin, such as the Coastal Cordillera, the Precordillera, the main Andean orogen, or the retro-arc fold-thrust belts (Fig. 1). This distribution is an expression of the complex, long-term interaction between a series of tectonic processes. These include first-order changes in the subduction system parameters leading to spatio-temporal shifts, stagnation or resumption of the arc magmatic focus, such as flat-slab and slab break-off episodes, crustal thickening and delamination events, trench retreat through slab rollback and collision of mid-ocean ridges or allochthonous terranes (Gianni et al., 2019; Mpodozis and Kay, 1992; Navarrete et al., 2019; Oliveros et al., 2019). The trench-arc configuration can also be modified bysubduction accretion/erosion and crustal denudation of the upper plate (e.g., Ramírez Arellano et al., 2012; Scholl and von Huene, 2010), or by tearings in the oceanic plate with back-arc volcanism related to slab windows (e.g., Pesicek et al., 2012).

* Corresponding author.
E-mail address: pablo.rossel@unab.cl (P. Rossel).

https://doi.org/10.1016/j.lithos.2020.105510
0024-4937/

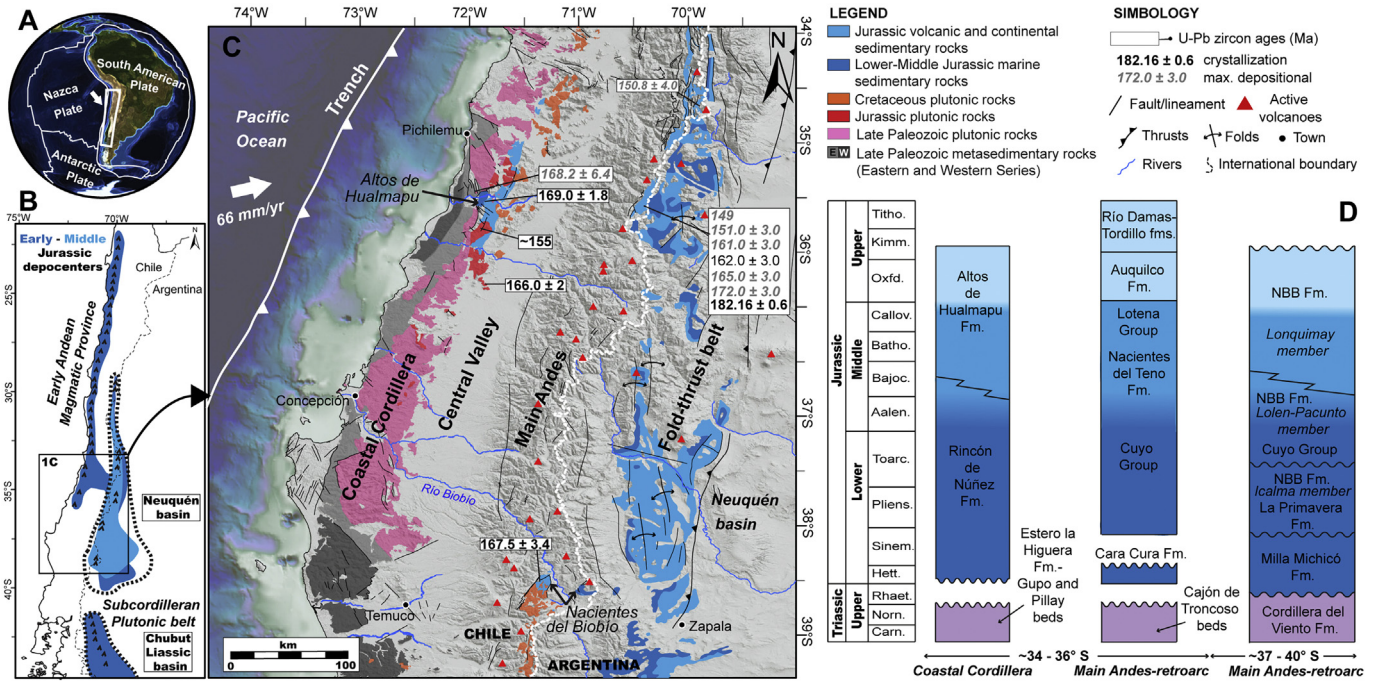

Fig. 1. A) A) Geotectonic setting of the Andean margin, with the eastward subduction of the Nazca plate beneath South America. B) Schematic distribution of the Jurassic magmatism from northern Chile to Patagonia, and the main depocenters associated with the retroarc marine and continental basins. C) Geological map showing basement and Jurassic units and their disposition in the different morphostructural domains. Modified after Sernageomin (2003) and Segemar (1995). D) Stratigraphic chart of Triassic-Jurassic units and correlations between both Andean slopes for the considered segment of the margin.

The inception of the Andean tectonic cycle during the Early Jurassic occurred partly simultaneous with the destabilization of the Pangea supercontinent and following the collapse of the Gondwana orogen, establishing a long-lasting orogenic and magmatic configuration of the margin (e.g., Charrier et al., 2007; Mpodozis and Ramos, 1989). The previous, "pre-Andean" Permian - Triassic stage, has been generally regarded as a period of quiescence/waning in arc magmatism with a dominance of within-plateactivity at these central Andean latitudes. (e.g., Mpodozis and Kay, 1992). However, this perspective has been recently challenged by proposals arguing for a subduction-related nature of most of the magmatic units in this zone, reflecting an uninterrupted subduction setting and continuous arc magmatism (e.g., Oliveros et al., 2019).This scenario has also been proposed in southern latitudes (~36–39°S), represented by several isolated calc-alkaline plutonic suites of Triassic age (e.g. Vásquez et al., 2011).

After this transitional stage, the beginning of Andean evolution along the margin took place under an extensional regime, where subduction magmatism evolved from mainly poorly differentiated suites associated with intra-arc and retro-arc basins. In the Central Andes margin, from northern to central Chile (~18–35°S), a remarkable continuous plutonic-volcanic association constitutes most of the Coastal Cordillera for at least 2500 km, composed of batholithic bodies and thick (>8000 m) volcanic sequences (La Negra, Ajial, Horqueta formations; Buchelt and Téllez, 1988; Emparan and Pineda, 2000). This magmatic association is characterized by I-type, mafic to intermediate composition with mostly calc-alkaline trends (Vergara et al., 1995; Kramer et al., 2005; Lucassen et al., 2006;) emplaced mainly under an extensional to transtensional tectonic regime (Grocott and Taylor, 2002; Scheuber and González, 1999), but with minor periodic transpressional events (Creixell et al., 2011; Ring et al., 2012).

Several petrological constrains have been made on these rocks, aided by the good preservation and exposure resulting from almost no weathering since the late Miocene (e.g., Lamb and Davis, 2003), leading to an integration of these units as the Early Andean Magmatic Province (EAMP, Kramer et al., 2005; Lucassen et al., 2006; Rossel et al., 2013). The relatively uniform compositional pattern of this complex is contrasted by the presence of enriched, OIB-like magmatic sources that formed back-arc associations between ~26–31° S, resembling characteristics of the actual western Pacific Island Arcs (Rossel et al., 2013).

To the south, in northern Patagonia (~41–45°S, Fig. 1), there are two plutonic associations that represent early Andean magmatism: the Late Triassic Batholith of Central Patagonia and the Early Jurassic Subcordilleran plutonic belt. They represent arc plutonism as I-type, calc-alkaline, mostly granitic suites (e.g., Gordon and Ort, 1993; Rapela et al., 1991; Zaffarana et al., 2014), whose magmatic focus migrated with a SW-clockwise pattern from the foreland toward the proto-Andean axis during the Jurassic (see Echaurren et al., 2017; Navarrete et al., 2019; Rapela et al., 2005), drawing a notorious deflection in the early Jurassic arc axis (Fig. 1). This magmatic pattern led to the establishment of a well-defined NS-striking belt since the Late Jurassic across Patagonia: the >1500 km long Patagonian Batholith (e.g., Hervé et al., 2007; Pankhurst et al., 1999).

Between these two regions (~35–41°S), there is a remarkable decrease in the exposure of Jurassic arc units, only represented by basic to intermediate intrusive and volcanic rocks in the eastern Cordillera de la Costa (Gana and Tosdal, 1996; Morel, 1981) and isolated volcanic/volcaniclastic rocks in the main cordillera (De La Cruz and Suárez, 1997. Interestingly, this segment is located to the west of the main depocenter of the Neuquén basin in Argentina (Fig. 1) which extends from the main cordillera toward the retro-arc and was suffering at that time its main stages of rifting and subsidence (e.g., Bechis et al., 2014; Tunik et al., 2010). Here, Jurassic volcanic activity is registered through ash-layers interbedded within the sedimentary infill (Junkin and Gans, 2019; Mazzini et al., 2010) and by bimodal volcanic rocks emplaced during the initial Early Jurassic extension (D'Elia et al., 2012; Llambías et al., 2007). While the pyroclastic rock association providesno reliable location for the axis of the Jurassic arc, the volcanic rocks possess a geochemical signature indicative of a back arc, asthenospheric origin (D'Elia et al., 2012; Llambías et al., 2007), hampering a detailed characterization of arc-related units, and hence, in making inferences regarding the margin dynamics.

The aforementioned scenario defines an enigmatic paleogeographic configuration, as it describes a first-order segmentation of the initial Andean arc at the latitudes of central Chile.

In order to interpret the prevailing tectonic processes and potential effects of pre-Andean segmentation into the early development of the Andean magmatic arc, we acquired new geochemical, geochronological and isotopical data along two critical areas at 35° and 39°S, between the present Coastal and Andean cordilleras. A petrogenetic characterization of these units (Altos de Hualmapu, Rincón de Núñez and Nacientes del Biobío formations) give insights of the slab-derived signature for the Jurassic volcanism and constrains its initial activity and tectonic setting.

1.1. Geological setting of Jurassic volcanic rocks

The Coastal Cordillera in central Chile (Fig. 1) is dominated by Late Paleozoic metamorphic complexes (Western and Eastern Series; Willner, 2005), which are intruded by the Carboniferous Coastal Batholith and by small epizonal Upper Triassic plutons (Vásquez et al., 2011). Older stratified rocks in this domain unconformably overlie the crystalline basement, corresponding to Upper Triassic volcanic, volcaniclastic and marine/continental rocks scattered as isolated depocenters with reduced areal distribution, part of the NW-SE striking Biobio-Temuco basin (see Charrier et al., 2007). In some regions, such as the Curepto Basin at 35°S, these Triassic sediments are covered by deep marine Hettangian-Sinemurian rocks of the Rincon de Nuñez Formation that progressively prograde to shallow marine deposits with higher proportions of epiclastic sediments (Corvalan, 1976).

In the Coastal Cordillera between ~32° and 34°S, Middle Jurassic volcanic activity is characterized by a geochemical arc signature rather similar to the northern EAMP but with a higher proportion of felsic effusive rocks (Vergara et al., 1995). This activity waned toward the Late Jurassic, synchronously with effusion of thick homogeneous sequences of volcanic material in the back-arc during Kimmeridgian to Tithonian (Creixell et al., 2011; Ring et al., 2012; Rossel et al., 2014) and preceding the Early Cretaceous re-establishment of the main arc in the Lo Prado Formation between ~33 and 34°S (e.g., Charrier et al., 2007).

South of 34°S, mainly through costal exposures, a series of small Late Triassic epizonal granitoids with a calc-alkaline signature intrudes the crystalline basement; these units probably represent the early reactivation of the Andean magmatic arc (e.g., Vásquez et al., 2011). There is an eastward migration of the parental magmatic focus of these rocks, as a strong subduction-related signature characterize the granitoids of the eastern Coastal Cordillera at 34°–37°S (Vásquez et al., 2011). In this area, volcanic activity coeval with the intrusive rocks have been reported as scattered sections, with intermediate to felsic Late Triassic volcanic rocks of the Estratos de la Patagua (36°S) and Crucero de los Sauces (35°S) and Santa Juana (37°S) formations (Abad and Figueroa, 2003; Corvalan, 1976), which are devoid of detailed geochemical and geochronological constrains.

It is possible to recognize Jurassic volcanic rocks in southern central Chile mainly at two localities (Fig. 1), the first at 35°S in the Coastal Cordillera of the Maule Region, represented by the Altos de Hualmapu Formation (Morel, 1981). This unit is mainly composed of tuffs, volcanic breccias, andesitic lavas and subvolcanic intrusives, and minor intercalations of marine sediments at the base. The second area is located at 38–39°S in the High Andes of Chile and Argentina and is represented by the lower, mostly basaltic and upper volcanic and volcaniclastic members of the Nacientes del Biobio Formation (De La Cruz and Suárez, 1997, Fig. 1). These units constitute the main focus of the present study.

1.2. Samples and methods

In order to characterize in detail the units studied, 36 samples of tuffs, lavas and subvolcanic bodies were collected to perform petrographic analysis; 22 where from the Altos de Hualmapu formation, 6 from the Icalma member and 8 from the Lonquimay member. Thin sections where prepared in Geochronos Ltda. and studied in the optical microscopy laboratories of the Universidad Andres Bello. 18 samples of lavas and subvolcanic rocks were selected to determine whole rock major and trace compositions following different criteria such as aerial distribution, stratigraphic position, and alteration degree. 10 of the previous samples were selected for Sr, Nd and Pb analysis. Finally three samples were selected for zircon U—Pb LA-ICP-MS geochronological analysis. Main features of studied samples are listed in Table 1. Additionally a database of 346 samples of the Jurassic Andean region of Chile and Argentina between 18° and 43°S has been compiled (Supplementary material X), in order to compare the magmatism represented by the samples analyzed in this work, along the entire Early Andean Margin.

1.3. Geochemical data

Major and trace element concentrations were determined using standard XRF and ICP-MS techniques (detailed in the Supplementary material) at Activation Labs in Ontario, Canada and in the Laboratorio de Analisis Elemental of the Universidad Andres Bello in Concepción, Chile. Rb, Sr, Sm and Nd were measured by isotope dilution on separate aliquots (see below) for isotope age correction. All samples had consistent trace elemental results between ICP-MS and isotope dilution TIMS data, evidently with the much higher precision of the isotope dilution technique. On the other hand, major elements measured by ICP-MS method in Universidad Andres Bello show inconsistent results especially in Al_2O_3 and SiO_2, so the last is not included in the result table and the whole set is not considered in the diagrams and the discussion.

All isotopic work was performed in the Radiogenic Isotope Facility at the University of Arizona. Isotopic separation was carried out in chromatographic columns via HCl elution. Conventional cation columns filled with AG50W-X4 resin were used for Rb,Sr and REEs separation and anion columns with LN Spec resin for Sm Nd separation (Drew et al., 2009). Isotopic analyses were performed using a VG Sector 54 thermal ionization mass spectrometer (TIMS) instrument fitted with adjustable $10^{11}\Omega$ Faraday collectors and Daly photomultipliers. NBS SRM 987 Sr standard and La Jolla Nd standard were analyzed during the sample run in order to ensure the stability of the instrument. Rb was analyzed on a single collector XSeries2 ICP-MS in solution mode, whereas Sm was analyzed statically on TIMS (Ducea and Saleeby, 1998). Pb was separated using SR spec columns and analyzed in solution mode on an ISOPROBE multicollector ICP-MS following the procedure in Drew et al. (2009). This procedure includes Th spiking for fractionation correction. NBS981 was used as an external standard.

1.4. U—Pb geochronology

Zircons were extracted from two tuffs and one epiclastic sandstone (HUAL-12, MIII2–01 and RACG-5.30 respectively) through crushing, milling, gravitational separation and heavy liquid treatment. At least 30 crystals were randomly selected (regardless of their size, form or colour) using a stereomicroscope; they were then mounted in 25 mm epoxy and polished. U—Pb geochronology of zircons was conducted by LA-MC-ICP-MS at the SERNAGEOMIN laboratories following the protocols of the laboratory. For more detailed information visit www.sernageomin.cl

2. Results

2.1. Field data and petrography

2.1.1. Altos de Hualmapu Formation

At 35°S, in the coastal range of Chile, the Altos de Hualmapu Formation overlies in slight angular unconformity the Hauterivian to Pleinsbachian clastic marine deposits of the Rincon de Nuñez Formation

Table 1
Main features of the studied samples included in this work. Pl: plagioclase. Fe—Ti Ox: Fe and Ti oxides. Px: pyroxene. Anf: Amphibole. Qz: Quartz. Bt: Biotite. Ep: epidote. Cc: Calcite. Chl: Chlorite. VLit: Volcanic lithics. Gls: Glass.

Sample	West coordinate	South coordinate	Rock type	Composition	Mineralogy	Alteration	Analysis
PA-2	71°18′50,2″	38°49′11,7″	Lava flow	Basalt	Pl + Fe-Ti Ox	Ep	WR chemistry and Sr-Nd-Pb isotopic measurements
MIII1–06	71°19′51,0″	38°49′09,6″	Lava flow	Basaltic andesite	Pl + Px	Chl, Cc	WR chemistry and Sr-Nd-Pb isotopic measurements
MII2–02	71°18′52,4″	38°27′25,7″	Lava flow	Basaltic andesite	Pl + Fe-Ti Ox+Anf	Ep, Cc	WR chemistry and Sr-Nd-Pb isotopic measurements
MIII2–02	71°20′36,9″	38°27′42,3″	Lava flow	Dacite	Qz + Pl + Fe-Ti Ox	Ep, Cc	WR chemistry and Sr-Nd-Pb isotopic measurements
MIII2–03	71°18′50,3″	38°27′26,7″	Lava flow	Dacite	Pl + Bt	Chl, Cc	WR chemistry
HUAL-01A	71°53′17″	35°08′42,1″	Lava flow	Andesite	Plg	Chl, Ep, Cc	WR chemistry
HUAL-04	71°50′58,3″	35°07′52,2″	Lava flow	Andesite	Pl + Cpx	Chl, Ep	WR chemistry
HUAL-06	71°52′11,7”	35°09′27,4”	Lava flow	Andesite	Pl + Cpx + Fe-Ti Ox	Chl, Ep	WR chemistry and Sr-Nd-Pb isotopic measurements
HUAL-09	71°51′12,3″	35°07′51,4″	Lava flow	Diabase	Pl + Ol + Cpx + Fe-Ti Ox	Cc	WR chemistry
HUAL-01b	71°52′05,4″	35°08′43,9″	Lava flow	Andesite	Pl	Chl, Ep, Cc	WR chemistry
CU-01	72°14′37,3″	44°03′34,1″	Subvolcanic bodie	Microdiorite	Pl + Cpx + Fe-Ti Ox	Cc	WR chemistry
CU-03	71°50′58,2″	35°03′33,1″	Subvolcanic bodie	Microgranodiorite	Pl + Cpx + Fe-Ti Ox	Chl, Ep	WR chemistry
HU-02	71°46′10,2″	35°02′47.9″	Lava flow	Rhyolite	Pl	Chl, Ep, Cc	WR chemistry and Sr-Nd-Pb isotopic measurements
HU-03	71°46′02,2″	35°02′56,8″	Subvolcanic bodie	Microdiorite	Pl + Cpx + Fe-Ti Ox	Chl, Ep	WR chemistry and Sr-Nd-Pb isotopic measurements
EST-02	71°50′21,3″	35°07′57,6″	Dique	Microdiorite	Pl + Cpx + Fe-Ti Ox	Chl, Ep	WR chemistry
RACJ-60	71°53′13,0″	35°08′54,1″	Subvolcanic bodie	Microdiorite	Pl + Cpx + Fe-Ti Ox	Chl, Ep	WR chemistry
RADICK1	71°53′17,4″	35°08′42″	Dique	Diabase	Pl + Cpx + Fe-Ti Ox	Cc, Chl	WR chemistry and Sr-Nd-Pb isotopic measurements
RADICK2	71°53′36,6″	35°08′23,8″	Dique	Diabase	Pl + Cpx + Fe-Ti Ox	Chl	WR chemistry and Sr-Nd-Pb isotopic measurements
HUAL-02	71°51′58,4″	35°08′31,9″	Lava flow	Andesite	Pl + Cpx + Fe-Ti Ox	Chl, Ep	WR Sr-Nd-Pb isotopic measurements
RACG-5.30	71°51′36,8”	35°10′00,4”	Epiclastic sandstone	Feldespatic	Pl + VLit	Chl, Ep	U-Pb Geochronology
HUAL-12	71°51′13,3″	35°07′51,4″	Tuff	Dacitic	Qz + Gls	CC, Chl, Ep	U-Pb Geochronology
MIII2–01	71°18′50,3″	38°27′26,7″	Tuff	Lithic	Qz + VLit	Chl, Ep	U-Pb Geochronology

Pl: plagioclase. Fe—Ti Ox: Fe and Ti oxides. Px: pyroxene. Anf: Amphibole. Qz: Quartz. Bt: Biotite. Ep: epidote. Cc: Calcite. Chl: Chlorite. VLit: Volcanic lithics. Gls: Glass.

(Corvalan, 1976) and underlies in apparent conformity with the continental volcanic Lower Cretaceous deposits of the Estratos del Patagual (Bravo, 2001). The studied unit is mainly composed of three lithologies:

2.1.1.1. Andesitic volcanic breccias. They are the dominant lithology in this unit that correspond to thick and massive levels (over 60 m) with no clear top or base, of volcanic breccias with large (sometimes over 50 cm) rounded to sub-rounded andesitic clasts in a purple to greenish andesitic matrix (Fig. 2a). Andesitic clasts in the breccia commonly show well developed plagioclase phenocrysts of 3 to 5 mm long axis, in a purple to reddish, sometimes greenish, aphanitic matrix.

2.1.1.2. Andesitic tuffs. They represent the second most abundant lithology and correspond to vitric and crystal tuffs composed mainly of plagioclase fragments and devitrified glass, minor mostly volcanic lithic clasts and clinopyroxene. All the constituents are partially or totally replaced by carbonate, chlorite and subordinately epidote. (Fig. 2b).

2.1.1.3. Andesitic lavas and subvolcanic bodies. Lavas are the least common lithology in the Altos de Hualmapu Formation and are apparently concentrated at the base of the unit intercalated with the previously described breccias. Compositionally, these are andesites with plagioclase phenocrysts (10–40%) of 0.1 to 2.8 mm, in a matrix of intergranular texture, composed mainly of plagioclase and minor amounts of clinopyroxene (augite) and Fe—Ti oxides (Fig. 2c). They are similar to the volcanic clasts recognized in volcanic breccias. Andesitic dikes and sills of 1 to 10 *m* in thickness of similar composition are commonly observed crosscutting the underlying Rincon de Núñez Formation (Fig. 2d) or previous deposits of the Altos de Hualmapu Formation. Petrographically, these dikes show the same textures than their effusive counterparts but with a coarser matrix. The porphyritic portion is dominated by plagioclases and sometimes few clinopyroxenes (augite) immersed in a matrix dominated by plagioclase and minor amounts of clinopyroxenes and Fe—Ti oxides (Fig. 2e).

2.1.2. Nacientes del Biobio Formation

At 38–39°S the Jurassic Nacientes del Biobio Formations have no observable base and underlies in angular unconformity the Cretaceous to Paleogene deposit of the Vizcacha-Cumilao volcano sedimentary complex and the continental deposits of the Oligo-Miocene Cura-Mallín Formation (De La Cruz and Suárez, 1997). This Formation has been divided into three members by De La Cruz and Suárez, 1997. a) A marine mostly basaltic lower member with small sedimentary intercalations (Icalma Member, Fig. 2f, 3a and b), b) a deep marine sedimentary middle member (Lolén-Pacunto Member) with no volcanic intercalations and c) an upper mostly subaerial volcanic member (Lonquimay Member) with marine intercalations at the base (Fig. 3c). Based on fossiliferous material recognized in the lower and upper members, and the intrusion of the Upper Jurassic to Upper Cretaceous plutonic bodies, previous authors suggest a Pliensbachian to Oxfordian age for the deposits of the Nacientes del Biobio Formation, but not clear age is available for the upper volcanic deposits.

2.1.2.1. Icalma member. Petrographically the Jurassic volcanism of the High Andes is dominated by basalts and basaltic andesites at the base. These lavas usually show pervasive propylitic alteration which most of the time completely obscures the primal features of the lavas (Fig. 3a and b). Mineralogy is dominated by plagioclases and lesser amounts of

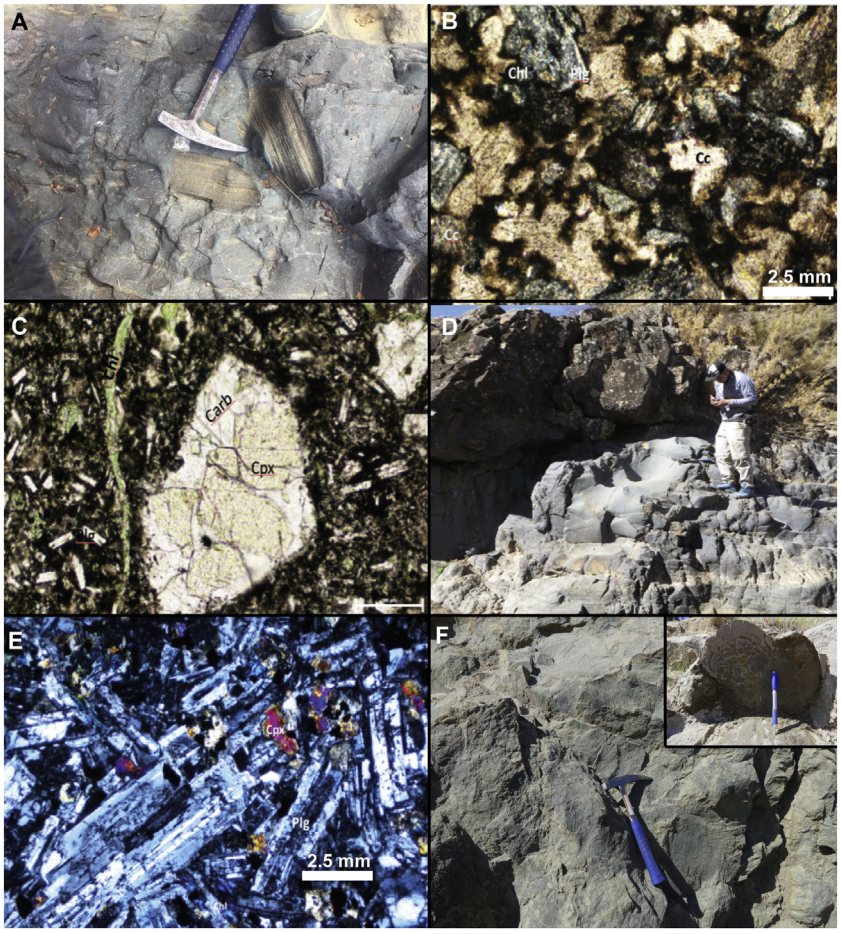

Fig. 2. Photographies and photomicrographies of the recognized Jurassic volcanic rocks. A) Sedimentary clasts in volcanic breccias of the Altos de Hualmapu Formation. B) Vitric tuff with a matrix highly altered to calcite and plagioclase clasts altered to chlorite of the Altos de Hualmapu Formation. C) Andesitic auto breccias with clinopyroxene crystals altered to calcite. D) Dacitic dyke crosscutting andesitic volcanic deposits of the Altos de Hualmapu Formation. E) Clinopyroxene-bearing microdiorite intruding the Altos de Hualmapu Formation. F) General view of pillow basalts of the Icalma member, Nacientes del Biobío Formation. Note the sandy clastic sediments between the pillows as light greenish materials. Inset in the top right is a detailed view of the pillow structures.

chloritized pyroxenes and completely iddingsitized olivines in an intersertal matrix mostly formed of plagioclase microlites with minor pyroxenes, olivines and Fe—Ti oxides as a mafic phase.

2.1.2.2. Lonquimay member. The volcanics of the upper member are composed mainly of crystalline to lithocrystalline tuffs and lapillites (Fig. 3d) with secondary intercalations of andesitic and dacitic lavas, which sometimes show clear evidences of flow (Fig. 3e). Tuffs are dominated by quartz and plagioclase fragmented clasts and lesser amounts of small andesitic and dacitic lithics (Fig. 3f). Vitric shards are almost absent but devitrified textures suggest that glass was an important constituent of the matrix. Lapillites are mostly composed of andesitic and dacitic clasts in a fragmental matrix composed of plagioclase, quartz, volcanic lithics and probably glass.

Lavas of the upper member range between andesites and dacites. The first show porphyritic texture with euhedral crystals of plagioclase in a matrix composed of an intersertal arrangement of plagioclases and glass. Small amounts of mafic minerals are observed and when present they correspond to Fe—Ti oxides and pyroxenes, locally conforming an intergranular texture with plagioclase. Dacites on the other hand show a clear fluidal texture (Fig. 3g) and are mainly composed of bands of devitrified glass intercalated with bands of small microliths of quartz and plagioclase. No alkali feldspars or mafic phases are observed.

2.2. Geochemistry

2.2.1. Major and trace element distribution

Major and trace element abundances for the studied volcanic and intrusive rocks are listed in Table 2. Below we first present description of geochemical results followed by a discuss of the effects of the secondary alteration process that affected some of the studied rocks.

2.2.2. Major elements

The contents of SiO_2 (on anhydrous basis) of the volcanic and plutonic rocks vary significantly between 45.90% and 73.16%. The subvolcanic rocks of the Altos de Hualmapu Formation have the most restricted and lower SiO_2 contents, 45.90 to 51.67% (Fig. 4a) and are systematically lower than their effusive counterparts. The alkali content of the rocks ranges from 1.18 to 8.75 wt% (oxide), and it increases the higher the content of SiO_2 but with two anomalous values, being the lowest and highest not related to the less and more evolved samples respectively. According to their SiO_2 and K_2O content, the studied rocks have low to medium K calc-alkaline affinity. The wt% of TiO_2, MgO and FeO^t varies from 0.45 to 1.10, 0.08 to 5.58 and 3.02 to 10.19, respectively and it decreases as fractionation advances. The Al_2O_3 content ranges between 13.63 and 26,83 wt%. It is important to note that if all available data is considered, no evident diminishing as fractionation proceeds is observed, but if plotted against samples with available silica content, fractionation of aluminous phases can be assumed. The systematic

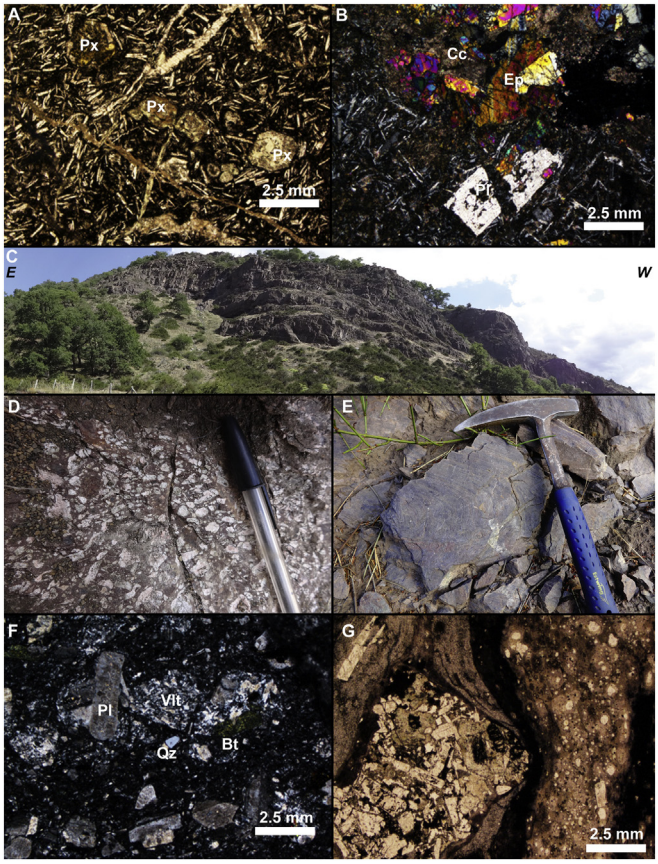

Fig. 3. Photographies and photomicrographies of the recognized Jurassic volcanic rocks. A) Basalt with intersertal texture and B) Basaltic andesite of clinopyroxene highly altered to epidote from the Icalma member. C) General view of the volcanic deposits of the Lonquimay member, Nacientes del Biobío Formation. Note that the upper limit is the present erosional surface. D) Pyroclastic deposits with abundant pumice clasts, part of the ignimbrite in the upper part of the sequence. E) Dacitic lava with flow structures in the Lonquimay member. F) Cineriticchrystalolitic tuff from the Lonquimay member. Note the presence of an andesitic volcanic clast in the dacite. F) Dacite with fluidal texture.

decrease in the contents of TiO_2, FeO, MgO, Al_2O_3 and CaO is compatible with progressive fractionation of Fe—Ti oxides, plagioclases, clinopyroxene and amphiboles which is consistent with the observed mineralogy in the studied rocks.

Chlorite, epidote and calcite are ubiquitous alteration mineral phases in the lavas, especially in rocks of the Nacientes del Biobio Formation; it occurs in fractures, amygdales or as cement in epiclastic sandstones and tuffs interbedded with lavas, probably as a result of over imposed metasomatism of later Cretaceous and Cenozoic plutonic bodies observed in the area (Belmar et al., 2004; De La Cruz and Suárez, 1997). The higher dispersion in the major elements vs silica and K2O/Na2O, FeOt/MgO and LOI vs Zr (Fig. 4a and b) of the samples of this unit is consistent with this scenario. In order to avoid the effects of element mobility in the analyzed samples, a Zr/Ti versus Nb/Yb classification diagrams is presented (Fig. 4c). The classification in terms of the more immobile elements confirms the sub-alkaline character of both units. Furthermore, even though the alkalis and CaO have the highest dispersion within the major elements, a trend of enrichment and depletion, respectively, is observed as SiO_2, or differentiation, increases.

In view of the presented results the major element content in the analyzed rocks are not recommended as proxies for petrogenetical interpretations, especially in rocks from Nacientes del Biobio Fm. and they should be used only as preliminary and not conclusive data.

2.2.3. Minor and trace elements

As observed in the multi-element diagrams (Fig. 5) all of the studied samples show enrichment in LILE compared to HFSE, relative to MORB. Additionally, the last group of elements shows concentrations that almost mimic those of the oceanic basalts, especially in less evolved samples. All the studied samples show negative Nb—Ta and Ti and positive Pb anomalies. Particularly, Zr show a negative though in most of the subvolcanic bodies and two lavas of Altos de Hualmapu Formation. Sr values are slithly more pronounced in Altos de Hualmapu Formation lavas respect to Nacientes del Biobio Formation samples. REE patterns show negative slopes ($La_n/Yb_n \approx$ between 2 and 3 with the exception of two samples with values over 5) with flat slopes in MREE to HREE ($Sm_n/Yb_n \approx 1$) and only one sample (HU-02) that shows an upward concave shape. Eu anomalies are almost absent from all the samples, with the exception of most evolved ones with a slight negative anomaly. Yb contents for all the samples are above 10 times the chondrite contents, with the exception of one lava sample of the Altos de Hualmapu Formation (Cu-03). Total REE contents (Table 2) range between 39.43 and 199.04 and highly correlates the SiO_2 and Zi/Ti contents.

LILE shows a greater dispersion than HFSE (Fig. 5) and, given the higher mobility of the former during the previously mentioned alteration processes, their usefulness in the interpretation of magmatic processes is limited and discussion on the genesis and characteristics of the magmas should be performed mainly using the HFSE and REE.

2.2.4. Isotopic ratios

The Sr–Nd–Pb isotope ratios of the studied samples are presented in Table 3 and are shown in Fig. 6. Data were recalculated to an initial ratio at 180 Ma for the Icalma member of the Nacientes del Biobio Formation and 165 Ma for the rest of the units. $^{87}Sr/^{86}Sr_{(i)}$ values for rocks of the arc domain range from 0.7035 to 0.7049. In general, the rocks from Nacientes de Biobio have completely overlapped values in relation to Altos de Hualmapu samples in terms of Sr. Initial Nd values range from 0,51,259 ($\varepsilon Nd = 3{,}50$) to 0,51,236 ($\varepsilon Nd = -1{,}3$). The Nacientes del Biobio samples show less enriched values with no negative epsilon values. With regard to Altos de Hualmapu Formation, samples from the intrusive counterpart are less radiogenic than the effusive rocks, but characterized by values always close to 0. Nd modal ages of all samples range between 0,57 to 1,03 Ga, with the exception of one sample from the Altos de Hualmapu Formation which has a value of 1,56 Ga.

Lead isotopic ratios have small dispersion, showing values that range from 18,56 to 18,94 for $^{206}Pb/^{204}Pb$, 15,65 to 15,72 for $^{207}Pb/^{204}Pb$ and 38,58 to 39,22 for $^{208}Pb/^{204}Pb$. No systematic variations between units can be observed.

2.2.5. U—Pb geochronology

The results of the three U—Pb dated volcanic rocks from the studied units are listed in Table 4 and shown in Fig. 7. Detailed information is available in the electronic supplementary material.

Sample MIII2–01, a lithocrystalline tuff located at the base of the volcanic deposits of the Upper member of Nacientes del Biobio yields two peaks of ages. The older, composed of 9 zircons gives a mean value of 312 ± 5.6 Ma. The younger peak gives a mean value of 167,5 ± 3.4 Ma based on 15 grains.

A tuffaceus sandstone from the top of the Rincon de Nuñez Formation (RACG-5,30) yielded a mean age of 177,0 ± 2,0 Ma and a maximum depositional age, based on three younger overlapping zircons, of ≈168 Ma. On top, a crystalline tuff in the middle section of the overlaying Altos de Hualmapu Formation yielded a mean age of 169,0 ± 1,8 Ma based on 17 grains.

Table 2
Major and trace element chemistry of U. Jurassic rocks in the studied area (oxides in wt%, trace elements in ppm).

Unit	Altos de Hualmapu													NBF (Icalma)		NBF (Lonquimay)		
Sample	HUAL-01A	HUAL-04	HUAL-06	HUAL-09	HUAL-01b	CU-01	CU-03	HU-02	HU-03	EST-02	RACJ-60	RADICK1	RADICK2	PA-2	MIII1–06	MIII2–02	MIII2–03	MII2–02
SiO2			59.83	45.90				73.16	55.33			51.67	47.00	50.29	54.31	63.38		55.76
TiO2	0.61	0.66	0.68	0.92	0.85	0.45	0.62	0.50	0.79	0.55	0.63	0.82	0.93	0.75	1.10	0.87		0.95
Al2O3	21.36	23.27	16.63	18.19	24.66	15.86	26.83	15.29	16.49	19.56	21.06	20.20	19.08	13.63	16.83	15.27		16.62
Fe2O3t	10.74	8.72	6.65	11.31	8.07	3.36	9.18	5.01	9.57	6.67	10.54	8.23	11.32	6.71	8.89	8.10		10.67
FeOt	9.66	7.85	5.98	10.18	7.26	3.02	8.26	4.51	8.61	6.00	9.48	7.41	10.19	6.04	8.00	7.29		9.60
MnO	0.13	0.12	0.12	0.16	0.10	0.09	0.11	0.01	0.16	0.10	0.17	0.16	0.19	0.15	0.12	0.17		0.19
MgO	3.48	2.67	2.59	5.58	4.47	0.89	3.32	0.08	1.50	2.45	4.05	3.00	5.36	4.72	4.34	1.69		2.32
CaO	6.47	9.19	5.36	6.82	9.35	2.08	9.45	0.17	12.43	2.36	5.20	7.99	10.06	14.25	4.99	2.10		2.19
Na2O	2.47	2.12	3.14	4.10	3.77	5.92	3.61	0.50	1.35	4.89	5.12	3.43	2.62	3.71	5.63	7.01		8.35
K2O	0.23	0.27	3.19	0.40	0.48	1.45	0.62	0.68	0.07	3.06	1.73	1.02	0.42	0.05	0.44	0.05		0.40
P2O5	0.29	0.30	0.19	0.13	0.12	0.12	0.17	0.09	0.20	0.36	0.34	0.22	0.18	0.13	0.19	0.31		0.16
Tot. Alk	2.70	2.39	6.33	4.50	4.25	7.37	4.23	1.18	1.42	7.95	6.85	4.45	3.04	3.76	6.07	7.06		8.75
LOI			1.40	5.94				3.60	2.44			3.22	3.05	5.89	3.39	1.29		2.30
Total			99.11	98.31				98.59	99.36			99.14	99.07	99.61	99.33	99.43		98.84
Rb	5.74	7.10	120.00	12.00	11.76	16.54	5.02	16.00	<2	103.04	29.67	24.00	11.60	0.50	5.00	<2	20.27	8.00
Cs	0.29	5.61	1.50	1.20	0.61	0.31	0.15	0.29	<0.5	1.27	0.37	1.40	0.74	0.12	0.50	0.19	0.37	0.80
Pb	8.86	8.99	18.00	3.16	3.69	30.55	9.24	4.21	12.00	31.10	5.84	20.66	5.22	5.92	8.00	18.00	12.67	21.00
Ba	138.26	116.84	627.00	222.00	120.75	408.57	157.59	263.00	36.00	657.42	449.87	397.00	179.27	21.00	206.00	56.00	265.40	158.00
Th	2.73	3.41	15.30	1.60	2.48	5.16	1.45	10.00	4.12	19.74	3.03	2.80	4.08	0.90	3.10	14.30	8.03	2.30
U	0.54	0.79	3.60	0.40	1.21	1.18	0.34	2.40	0.70	4.55	0.72	0.70	0.41	0.90	0.60	3.80	3.46	0.80
Nb	3.13	4.52	7.00	1.00	2.27	5.73	1.04	4.00	2.00	6.84	3.56	3.00	1.28	1.00	4.00	6.00	6.58	3.00
Ta			0.50	<0.1				0.30	0.20			0.20		0.10	0.20	0.50		0.20
Sr	414.96	267.40	317.00	461.00	435.01	123.04	556.97	181.00	473.00	474.06	393.19	473.00	409.62	187.00	306.00	356.00	167.24	133.00
Zr	91.52		247.00	48.00	71.56	186.45	51.64	172.00	78.00	258.17	122.04	86.00	49.54	53.00	133.00	239.00	315.20	78.00
Hf	1.27		5.80	1.20	6.61	4.79	0.04	4.70	2.10	6.61	2.23	2.30	0.88	1.20	3.10	6.10	7.46	2.10
Sc	21.39	25.94	18.00	37.00	39.33	14.43	24.17	8.00	24.00	14.77	21.32	20.00	30.58	29.00	29.00	21.00	11.59	34.00
V	248.74	256.11	142.00	371.00	309.95	13.81	254.47	92.00	247.00	39.91	146.58	159.00	311.69	240.00	244.00	85.00	300.53	73.00
Cr	20.85	28.40	50.00	30.00	70.38	67.32	28.51	40.00	60.00	21.08	47.63	20.54	15.92	230.00	40.00	<20	19.95	<20
Ni	24.02	20.41	40.00	9.49	27.52	69.10	27.99	50.00	60.00	21.29	16.29	15.55	15.65	80.00	50.44	<20	3.27	<20
Zn	90.57	68.65	70.00	80.00	79.62	128.29	54.54	<30	30.00	66.33	80.64	80.00	66.48	40.00	70.00	110.00	76.89	50.00
Y	24.23	20.99	25.00	15.00	13.59	32.87	13.65	12.00	18.00	29.61	21.98	21.00	16.57	14.00	22.00	42.00	25.34	19.00
La	13.96	14.05	30.00	10.00	6.77	27.66	8.34	27.00	12.90	34.94	14.77	13.60	10.00	4.90	15.80	23.60	29.00	9.20
Ce	32.92	33.71	63.70	22.70	17.34	64.34	19.51	54.00	29.60	80.40	34.74	30.90	22.90	11.90	35.00	55.40	54.79	21.40
Pr	4.95	4.87	7.76	2.99	2.93	8.83	3.18	5.59	3.84	10.10	4.98	4.05	3.12	1.70	4.45	7.05	6.45	2.94
Nd	19.62	19.34	30.60	13.90	10.88	36.38	12.13	21.00	17.10	40.31	19.66	18.10	14.70	8.10	18.20	30.10	25.13	13.20
Sm	5.56	5.32	6.40	3.90	3.67	8.48	3.96	3.80	4.10	8.96	5.37	4.30	3.90	2.10	4.30	7.60	5.13	3.30
Eu	1.44	1.31	1.37	1.12	1.06	1.87	1.10	0.83	1.22	1.99	1.53	1.43	1.20	0.74	1.37	1.65	1.50	1.01
Gd	4.76	4.43	5.50	3.50	2.79	7.24	3.06	2.40	3.90	7.43	4.64	4.40	3.70	2.60	4.70	7.60	4.97	3.80
Tb	0.79	0.70	0.90	0.50	0.46	1.09	0.44	0.30	0.60	1.00	0.69	0.70	0.60	0.40	0.80	1.30	0.80	0.70
Dy	4.32	3.83	4.90	3.10	2.75	6.02	2.53	2.00	3.60	5.39	3.97	4.20	3.20	2.70	4.60	7.70	4.66	4.00
Ho	0.95	0.79	1.00	0.60	0.56	1.28	0.53	0.40	0.70	1.10	0.84	0.80	0.60	0.60	0.90	1.60	0.99	0.80
Er	2.54	2.25	2.80	1.70	1.65	3.85	1.48	1.40	2.20	3.32	2.44	2.40	1.80	1.60	2.80	4.60	2.93	2.30
Tm	0.38	0.32	0.43	0.27	0.24	0.56	0.19	0.24	0.32	0.46	0.35	0.36	0.27	0.24	0.43	0.67	0.45	0.33
Yb	2.30	2.05	3.00	1.80	1.61	3.82	1.38	1.70	2.00	3.18	2.36	2.50	1.80	1.60	2.80	4.40	2.99	2.10
Lu	0.32	0.27	0.47	0.26	0.26	0.56	0.20	0.26	0.30	0.47	0.35	0.37	0.26	0.25	0.42	0.69	0.46	0.32
ΣREE	94.81	93.24	158.83	66.34	52.96	171.98	58.04	120.92	82.38	199.04	96.71	88.11	68.05	39.43	96.57	153.96	140.23	65.40

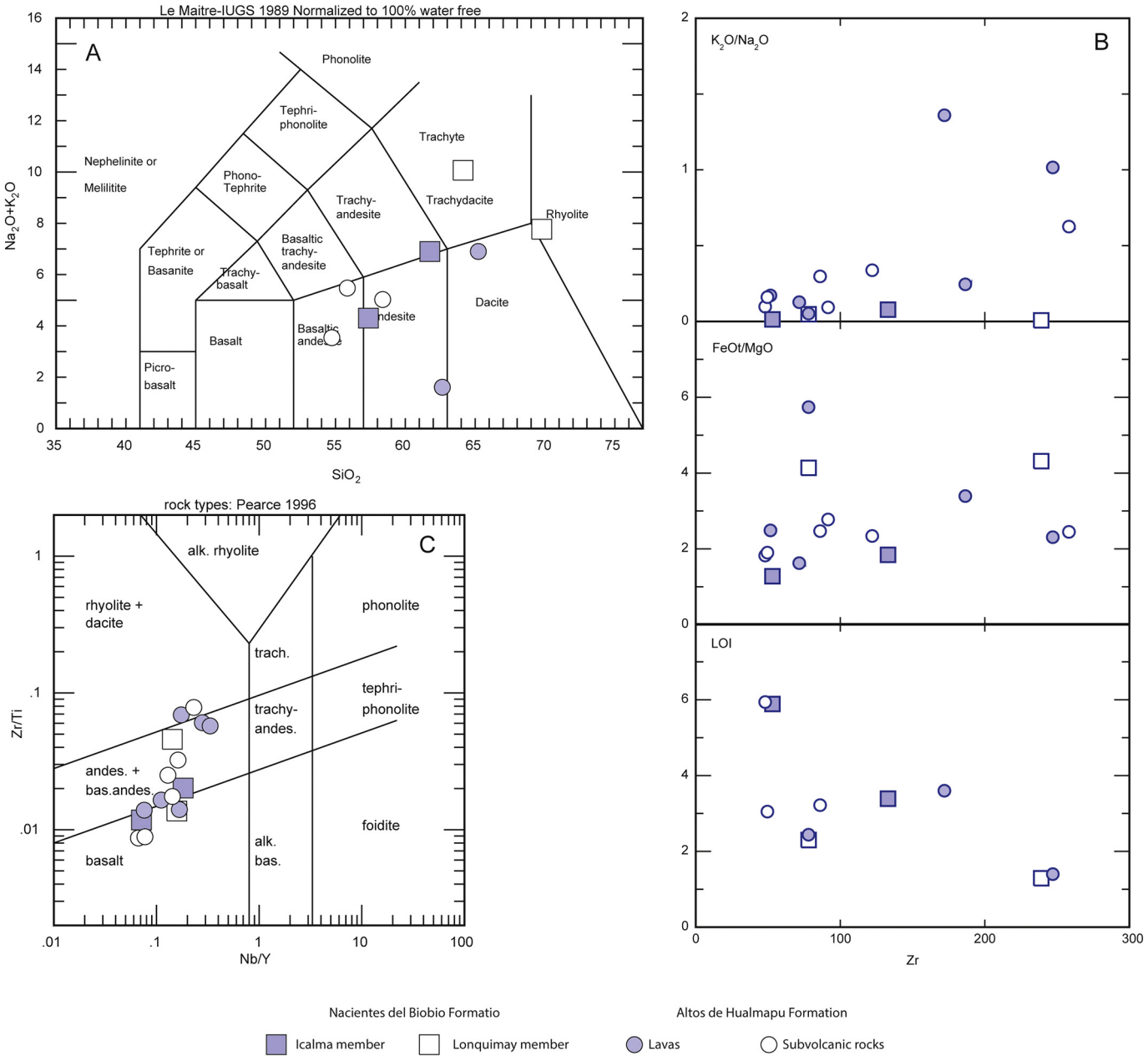

Fig. 4. Total alkalis versus silica (TAS; LeMaitre, 1989) and Nb/Y versus Zr/Ti classification diagram for altered volcanic rocks (Pearce and Wyman, 1996).

3. Discussion

3.1. Spatio-temporal constrains of Jurassic magmatism in the Southern Andes

The apparent lack of subduction-related magmatism along the southern Central and southern Andes margin (e.g., Mpodozis and Kay, 1990) has been recently re-interpreted as part of episodic Late Triassic-Early Jurassic pulses under continuous oceanic plate subduction (e.g., Oliveros et al., 2019; Vásquez et al., 2011).

Even though better represented by the Early Andean Magmatic Province in northern Chile (Kramer et al., 2005; Lucassen et al., 2006), two major episodes of magmatic arc activity can be recognized when correlating plutonic and volcanic rocks at a regional scale between ~34° and 39°S: an older Early Jurassic event formed by two short-lived pulses between ~200–195 Ma and ~185–180 Ma, separated by a magmatic waning/quiescence, with a younger, more widely developed Late Jurassic - Early Cretaceous magmatism (~160–140 Ma; Fig. 8; Vásquez et al., 2011; Oliveros et al., 2019)

Evidence for the first small event in the studied area are two isolated outcrops of alkaline and S-type like granites in the Coastal Cordillera at 35°S and 36°S (Vásquez et al., 2011), and the volcanic and subvolcanic deposits of the Cara Cura (36°S) and Milla Michico (37°S) formations, in western Argentina (Llambías et al., 2007; Drosina et al., 2017. For the second small pulse, no outcrops can be observed in the Coastal Cordillera, while at the axial Andean zone, in the Icalma area at 39°S, the Lower Icalma member of Nacientes del Biobio and the La Primavera Formation can represent this short-lived episode (De La Cruz and Suárez, 1997; Llambías et al., 2007).

Considering the location of the granites, the uncertainty of the age of the alkaline granite (based only on two zircon grains that roughly overlap in age; Vásquez et al., 2011), and the major geochemical differences with the apparently synchronous volcanic rocks to the east, we envisage that these plutonic rocks are probably part of the spatially related Late

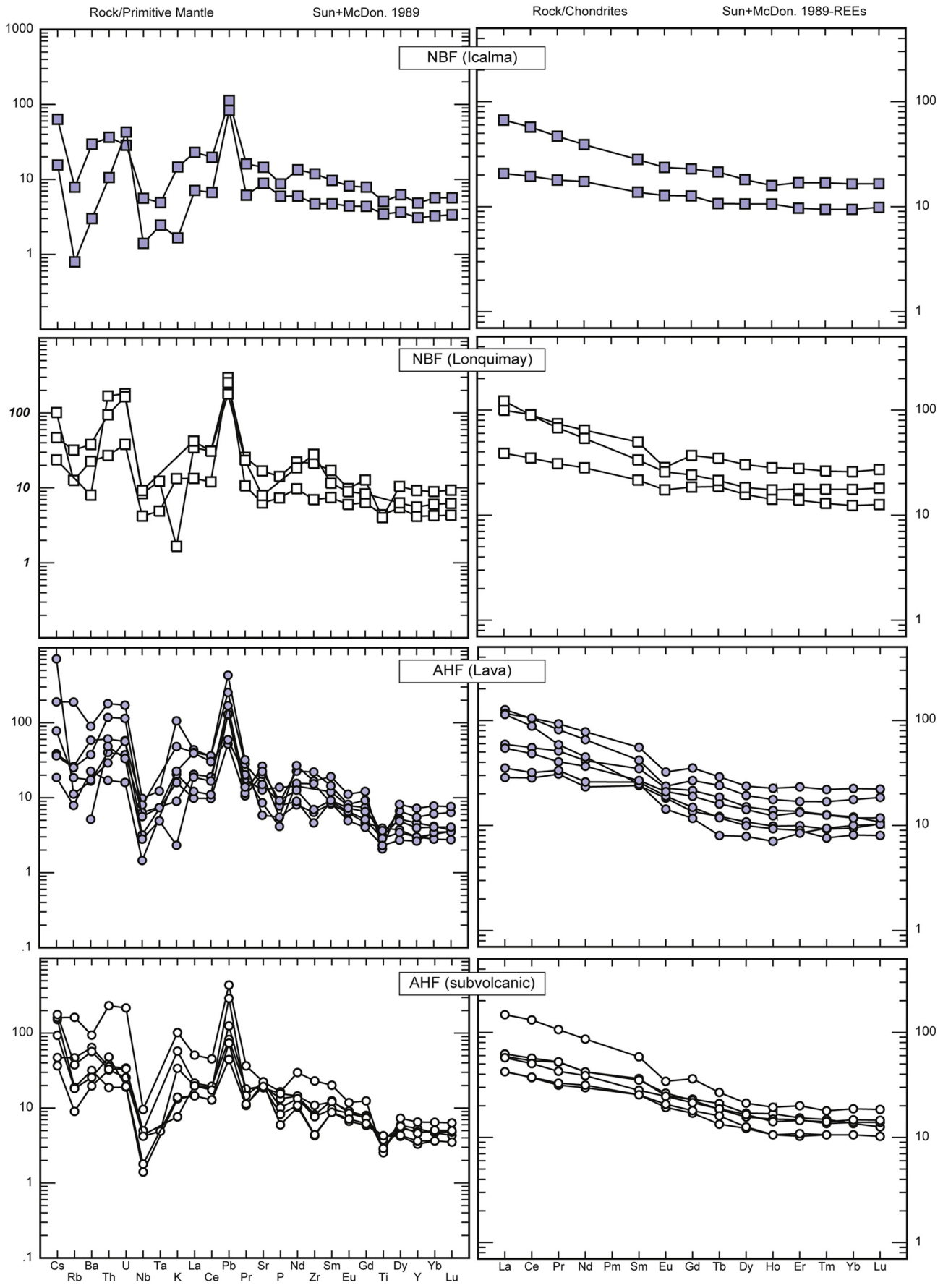

Fig. 5. MORB-normalized trace elements (Left) and Chondrite-normalized REE (Right) patterns for volcanic rocks of the studied units between 35° and 40°S. Normalizing values are from Sun and McDonough (1989).

Table 3
Sr, Nd and Pb isotopic composition of Jurassic igneous rocks in the studied units. εNd values are calculated as deviations from a chondritic uniform reservoir in part per 10^4, using present-day values of $^{143}Nd/^{144}Nd = 0.512638$ and $^{147}Sm/^{144}Nd = 0.1967$ (Faure, 1986; Wasserburg et al., 1981). Ages of rocks are from samples dated in this work.

Sample	Age (Ma)	87Sr/86Sr	87Sr/86Sr(i)	143Nd/144Nd	143Nd/144Nd(i)	eNd	eNd(i)	TMD	206Pb/204Pb	207Pb/204Pb	208Pb/204Pb
PA-2	180	0.7047	0.7047	0.51279	0.51259	3.0	3.5	1.03	18.75	15.70	38.81
MIII1–06	180	0.7048	0.7047	0.51269	0.51253	1.0	2.4	0.70	18.65	15.68	38.77
MIII2–02	168	0.7044	0.7044	0.51271	0.51255	1.4	2.5	0.78	18.83	15.69	38.96
MII2–02	168	0.7052	0.7049	0.51265	0.51248	0.1	1.1	0.99	18.56	15.65	38.58
HUAL-06	169	0.7069	0.7047	0.51259	0.51247	−0.9	0.8	0.74	18.80	15.67	38.92
HU-02	169	0.7049	0.7044	0.51263	0.51252	−0.1	1.9	0.57	18.94	15.72	39.22
HU-03	169	0.7047	0.7046	0.51260	0.51236	−0.8	−1.3	0.74	18.69	15.68	38.80
RADICK1	169	0.7050	0.7047	0.51264	0.51248	0.0	1.1	0.93	18.82	15.72	39.04
RADICK2	169	0.7044	0.7035	0.51270	0.51248	1.2	1.2	0.63	18.77	15.72	38.97
HUAL-02	169	0.7037	0.7037	0.51265	0.51246	0.3	0.7	1.56	18.82	15.70	39.00

Triassic magmatism in the area, and are not associated with the Jurassic volcanism in the Argentinean Precordillera.

On the other hand, given the age, location and subduction-related signature of the easternmost chain, it can be correlated with the Subcordilleran plutonic belt to the southformed by mostly I-type, calc-alkaline granitoids and minor gabbro that were emplaced under an extensional regime in the Chubut Liassic basin (e.g., Gordon and Ort, 1993; Rapela et al., 2005; see Fig. 1b).

The second, Middle-Late Jurassic to Early Cretaceous pulse is probably the manifestation of the definitive instauration of the "mature" Andean magmatic arc, considering that its volume is significantly higher than the one observed in the previous units of the areas, with a thickness of 4000–6000 *m* of volcanic and volcanoclastic sediments (Vergara et al., 1995; Wall et al., 1996). The latter values are within the volume range of effused material observed in other contemporaneous arc-related units in northern Chile, such as the La Negra Formation and the Agua Salada Volcanic Complex (Buchelt and Téllez, 1988; Emparan and Pineda, 2000).

This activity is correlated with the main pulse of volcanism of the Lago la Plata-Ibáñez Formation in the main Andes between ~41° and 46°S, which is made of thick sections of volcanic and volcanoclastic rocks with bimodal composition(e.g., Bruce, 2001; Echaurren et al., 2017; Suárez et al., 1999). Radiometric dating constrains this activity to ~155–138 Ma (U—Pb, Pankhurst et al., 2003; Suárez et al., 2009) and it is most likely cogenetically related to granitoids of the North Patagonian Batholith dated in ~160–150 Ma (U—Pb, Castro et al., 2011; Aragón et al., 2011). In this context, the ages here presented seem to have a good correlation with the magmatic activity observed in the entire Chilean margin.

The younger age obtained at the top of the sedimentary Rincon de Nuñez Formation (RACG-5,30) shows only one peak with a mean value of 177,0 ± 2,0 Ma, with half of the measured grains being younger than 180 Ma. These ages probably resemble the magmatic activity of the arc located to the east during this period, in current western Argentina suggesting a paleo fore arc position for this sedimentary unit.

Considering the overlap between the maximum deposition age of the previous sample and the mean age of a tuff located in the middle section of the overlying Altos de Hualmapu Formation, added to the presence of marine sediments at the base of the volcanic unit, suggest that the transition from marine sedimentation to subaerial volcanism during the middle Jurassic was progressive and without sedimentary gaps.

To the south, at 39°S, the base of the Nacientes del Biobio Formation has fine, sedimentary, clastic sequences intercalated between basaltic lava flows, characterized by a late Pliensbachian-Early Toarcian marine fossiliferous content (De La Cruz and Suárez, 1997). This age is consistent with the detrital zircon provenance data in the sampled Lonquimay member (sample MIII2–01, Fig. 7), as suggested by two zircon grains of ~190 Ma that would constitute a volcanic northern counterpart of the Subcordilleran Plutonic belt.

Maximum depositional age in sample MIII2–01, located at the base of the upper member of the Nacientes del Biobio Formation, is very similar, and overlaps with the age of the volcanism of the Altos de Hualmapu Formation, suggesting that the instauration of the main pulse of magmatism in southern central Chile and Patagonia was, at least, partly synchronous in this segment of the margin.

Otherwise, the new available geochronological data still suggest an almost complete absence of a magmatic record between 155 and 140 Ma in the Coastal Cordillera, south of 30°S. This magmatic gap is synchronous with the presence of large volumes of andesitic "back-arc" volcanism of the Rio Damas Formation in the Main Cordillera, between 33 and 35,5°S (Fig. 9; Rossel et al., 2014).

This lull of arc magmatism in the Coastal Cordillera is preceded by a transpressive stress regime registered in different sectors of the Chilean fore arc (Creixell et al., 2011; Ring et al., 2012; Rossel et al., 2014) as well as in the Argentinean retro arc and Main Andes, the latter represented by an EW-striking intraplate contractional belt (Huincul High; Naipauer et al., 2012). According to Navarrete et al. (2016), this contractional episode would have been a part of a wider scenario, characterized by a major Jurassic mantle overturn, the silicic outburst of the Chon Aike LIP (Pankhurst et al., 1998), and the N-directed ridge push product of the initial Wedell Sea opening and southward drift of South America, ultimately producing a thermal weakening of the lithosphere. However, the connection between this contractional episode and the waning of arc magmatism in the Coastal cordillera remains unclear.

In this sense, recent numerical models of subduction zone magmatism and plate dynamics can help unraveling the observed scenario for the Jurassic magmatism in the Southern Andes. The model of Magni (2019) suggest that magmatism in extensional back-arc environments, related to slab roll-back episodes, could inhibit the activity in the arc front and reduce the volume of magmatism, as depleted subcontinental mantle beneath the back arc domain is transported toward the arc zone by the mantle flow, being no longer able to produce melts in the arc front. This model can reproduce in a simple way the apparent lack of late Middle-Late Jurassic magmatism between 32 and 35°S, after effusion of the Horqueta volcanism in the Coastal Cordillera (Vergara et al., 1995) and subsequent generation of Rio Damas - Tordillo depocenters and related volcanism in the present Chile-Argentina boundary.

In this context we propose that, after the instauration of the Middle Jurassic arc, and after transpressive events recorded during Middle Jurassic in Coastal Cordillera (Creixell et al., 2011; Ring et al., 2012) a new extensional episode take place mostly during late Jurassic. This event was clearly recorded in back-arc clastic deposits of the Rio Damas and Tordillo formations (Mescua et al., 2008), and was provably related to roll-back of the slab that could induce a waning in the production of arc magmatism in the Coastal Cordillera of Central Chile synchronously with the progressive thining of the crust in back arc area that finally provoked the effusion of volcanic rocks in the high cordillera at the same latitudes (Rossel et al., 2014).

This event should have taken place mainly between ≈156 and, at least, 146 Ma, coinciding with the gap between the last available

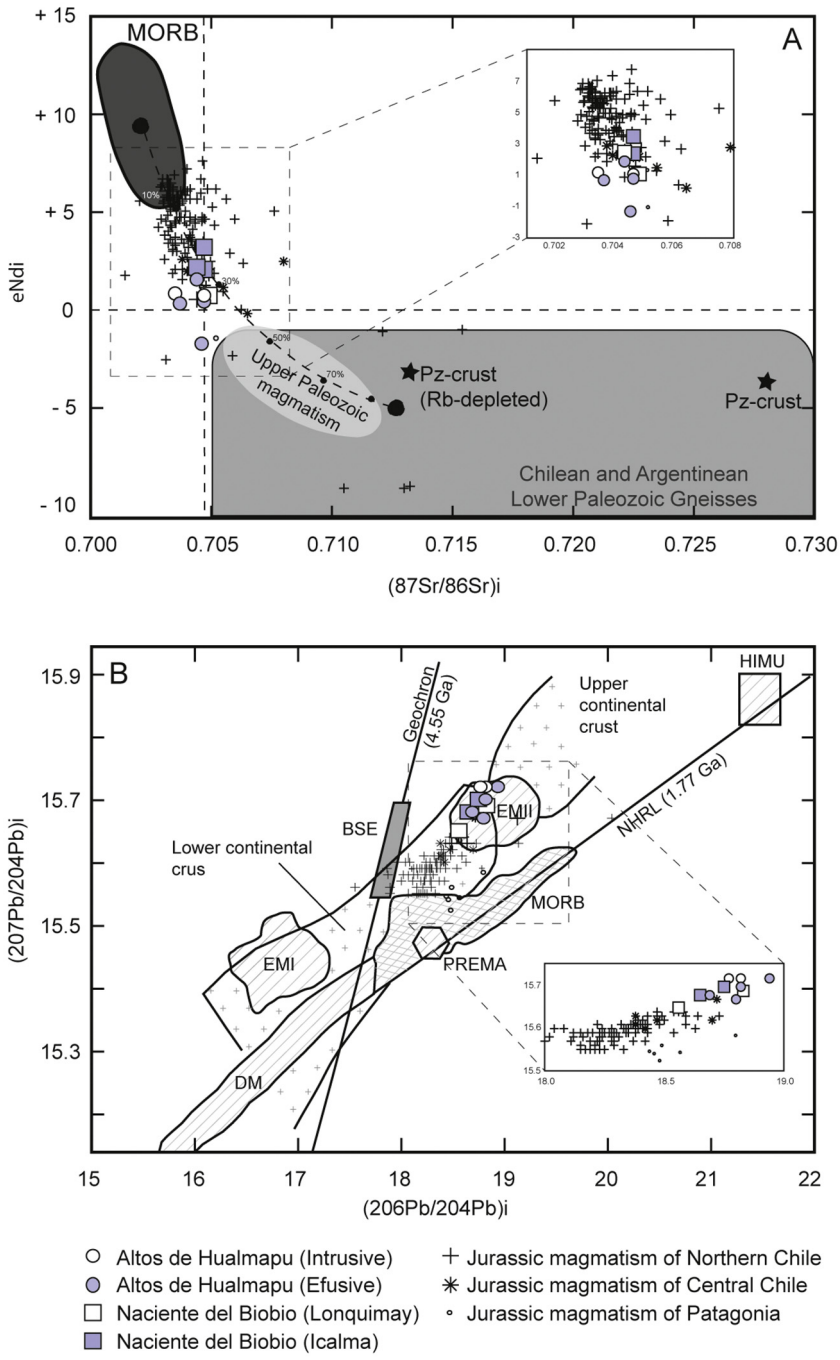

Fig. 6. A) $^{87}Sr/^{86}Sr$ versus εNd initial values from samples of the studied units between 35° and 40°S. BSE: Bulk Silica Earth. Ages corrected for in situ decay at 180 for the Icalma member of Nacientes del Biobio Formation and 165 Ma for the Lonquimay member of Nacientes del Biobio Formation and Altos de Hualmapu Formation. MORB is actual MORB corrected for in-situ decay considering 165 Ma. Dashed line shows mixing between MORB and Average Paleozoic Crust (Av. Pz Crust) after Lucassen et al. (2006). B) $^{207}Pb/^{204}Pb$ versus $^{206}Pb/^{204}Pb$ initial isotopic ratios for igneous rocks of the studied area between 35° and 40°S. Northern Hemisphere Reference Line (NHRL) after Hart (1984). Other Jurassic samples plotted in the diagram after references in Supplementary material X.

in-situ U—Pb age in the Coastal Cordillera and the maximum deposition age of *syn*-extensional deposits of the Rio Damas-Tordillo formations (Naipauer et al., 2015; Rossel et al., 2014).

After this stage of rifting, thermal subsidence should have led to a massive marine ingression during the Tithonian and Lower Cretaceous, represented by marine sediments observed from the Coastal Cordillera

Table 4
Resume of the U–Pb geochonological data from this study.

Sample	Unit	zircon type	n	WMA (Ma)	Max. Dep. Age (Ma)	Main peak (Ma)	Other peaks (Ma)
RACG-5.30	Rincon de Nuñes Formation	detrital	30	n/a	≈167	177.0 ± 2,0	n/a
HUAL-12	Altos de Hualmapu Formation	magmatic	17	169,0 ± 1,8	n/a	n/a	n/a
MIII2–01	Icalma member (NBB)	detrital	24	n/a	≈161	167,5 ± 3,4	312,3 ± 5,6

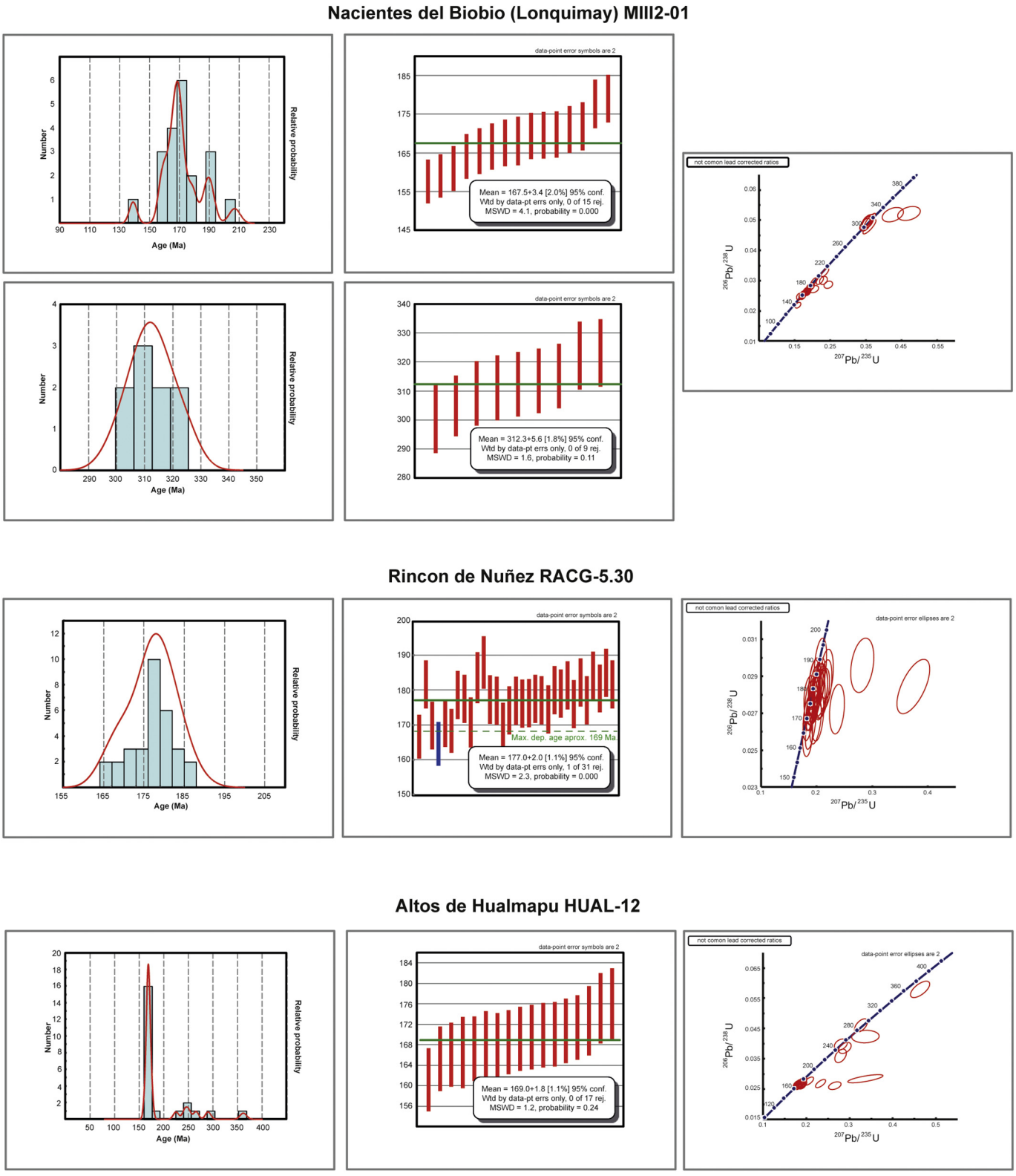

Fig. 7. Obtained U—Pb geochronological data. From left to right: probably density histograms then mean calculated age and finally concordia diagrams for three analyzed samples.

to the high Andes and the Argentinean retro arc (Lo Prado, Lo Valdes and Vaca Muerta Formations) covered to the west by a thick pile of volcanic rocks (and related intrusive bodies) of the so called Lo Prado Arc in the Coastal Cordillera of Central Chile (Fig. 9; Charrier et al., 2007).

3.2. Compositional constrains on Jurassic Arc magmatism

Jurassic magmatism is mostly mafic to intermediate subalkaline. Geochemical and petrographic characterization of Jurassic volcanic rocks in southern central Chile show a continuous compositional

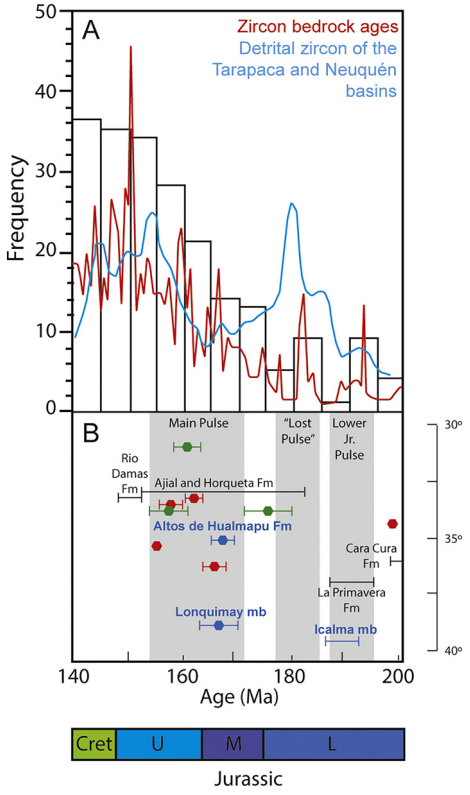

Fig. 8. A) Frequency distribution histogram for mineral U—Pb and K—Ar (Ar—Ar) radiometric ages from rocks of northern Chile (20°–30°S) and model distribution of detrital zircon U—Pb ages Jr. rocks of the Neuquén and Tarapacá back-arc basin. Modified after Naipauer et al., 2015 and Oliveros et al., 2019. B) Ar—Ar and U—Pb ages vs latitude (°) compilation for Jurassic magmatism in southern central Chile and Western Argentina between 30° and 40°S. Data from This work (blue); Creixell et al., 2011and Ring et al., 2012 (Ar-Ar; Green); Vásquez et al., 2011and references therein (Zircon U-Pb; Red). Black brackets are for estimated stratigraphic position after references in the text.

spectrum that ranges from basaltic andesites to dacites, except for the basal Nacientes del Biobío samples that exhibit a narrow compositional spectrum form by exclusively basalts and basaltic andesites (Fig. 4).

Trace elements distribution shows typical subduction related features such as Nb (Ta) and Ti depletions (Pearce, 1983) while the absence of Eu anomalies and plagioclase as a ubiquitous mineral in all samples suggest an already oxidized parental melt, consistent with the behavior of other elements in the context of subduction related environment. Zr vs Y diagram suggest a transitional behavior between tholeiitic and calc-alkaline (Fig. 10a), whereas Nb/Yb vs Th/Yb and Hf/3-Th-Nb/16 diagrams (Pearce, 1983; Wood, 1980) confirm a subduction related affinity for all the rocks (Fig. 10b and c).

Sr/Y, La/Nb and Nb/Yb (Fig. 11) ratios in most primitive samples (Basalts to andesites) show higher values than other Jurassic arc units in northern Chile and Patagonia (Echaurren et al., 2017; Kramer et al., 2005; Lucassen et al., 2006; Rossel et al., 2013), suggesting a possible enrichment of the source in the area. All samples show negative slopes in REE patterns with flat, almost horizontal HREE and values that range from 10 to 30 times the chondrite compositions (Fig. 5), suggesting the absence of garnet as residual phase in the source or depth crystallization. Additionally, all patterns show a subparallel shape with an increase in ΣREE with differentiation suggesting an evolution via fractional crystallization. A group of samples, the four most differentiated, show higher La/Sm ratios, which can be interpreted as enrichment probably via crust assimilation during crystallization.

La/Yb and La/Sm ratios have similar values for all the Jurassic Arc, but Sm/Yb values for Altos de Hualmapu Formation tend to be some of the highest (Fig. 11), whereas the Icalma member of Nacientes del Biobio Formationhas some of the lowest ones. Since the Icalma member basalts are the oldest samples in the set, this could reflect the immature nature of the earlier Jurassic Arc. Finally, one sample (HU-02) shows an upward concave shape, depleted in MREE (Tb, Dy and Ho; Fig. 5). This is the most evolved sample in the set and this feature could be related to an important influence of amphibole fractionation as a result of a progressive increase in water concentration during late crystallization. However, since no evidence of amphibole is observed in petrography of the volcanites this hypothesis should be taken carefully.

Estimated crustal thickness based on proxies of Mantle and Collins (2008) and Paterson and Ducea (2015), for the Early Andean Arc seems to be systematically under 40 Km which is consistent with the mostly extensional conditions mentioned before as observed in other arcs (Christensen and Mooney, 1995).

Previously mentioned characteristics are common features of magmatic systems that transit from early to mature stages of evolution (Chapman et al., 2017).

Isotopic values of Jurassic samples of Central Chile (34–35°S) show some of the enriched compositions when compared with the rest of the contemporaneous arc (Fig. 6, 11d, e and f). The origin of this isotopic and trace element enrichment seems to suggest particular conditions in the area that can be related to the interaction of two main endmember process/features according to available tectonic information: (i) Transpressional Middle Jurassic tectonics (Creixell et al., 2011; Ring et al., 2012) that enhance magma residence resulting in additional crustal contaminations and/or (ii) Local mantle heterogeneities and/or dynamics in the area that result in the melting of an enriched source (ei. Flat slab systematics in Patagonia; Navarrete et al., 2019).

$^{87}Sr/^{86}Sr_{(i)}$ vs $^{143}Nd/^{144}Nd_{(i)}$ mixing curve (Fig. 6a) suggest degrees of assimilation of Paleozoic crust in the range of 25 to 30%, which is inconsistent with the reduced distribution of the transpressive events recorded in central Chile, the mostly extensional behavior of the back arc during the Jurassic (Mescua et al., 2008; Mpodozis and Ramos, 1989), the estimated thickness of the crust based on geochemical proxies (~40 km) and the non-systematic higher isotopic enrichment in most evolved samples (Fig. 12).

Considering the above, even when crustal assimilation cannot be ruled out completely from the petrogenetic history of the magmas, the more plausible scenario is that other magmatic sources, such as a slab-derived contribution or particular mantle heterogeneities in the area (D'Elia et al., 2012; Llambías et al., 2007) influenced the observed nature of the studied lavas.

3.3. Tectonomagmatic model

At a regional scale along the Chilean margin, the Jurassic tectonomagmatic scenario has been characterized from igneous rocks that crop in northern Chile (Buchelt and Téllez, 1988; Kramer et al., 2005; Rossel et al., 2013; Scheuber and González, 1999), central Chile (Creixell et al., 2011; Rossel et al., 2014; Vásquez et al., 2011; Vergara et al., 1995), Patagonia and Antarctic Peninsula (Rapela et al., 1991; Gordon and Ort, 1993; Zaffarana et al., 2014; Riley et al., 2016; Craddock et al., 2017; Echaurren et al., 2017; Navarrete et al., 2019). However, a systematic comparison between these contemporaneous units is lacking, and the striking discontinuity of the Jurassic arc front at ~37–38°S has not been integrated within the early stages of Andean evolution.

These differences in the arc position suggest an unstable behavior of the slab under the continent., When taking into account the tectonic scenario recently proposed by Navarrete et al. (2019) for the Patagonian margin, where a Late Triassic flat slab configuration was followed by a slab detachment and roll-back since Early Jurassic time, it is reasonable to expect at least an slight perturbation/remobilization/convection of the subcontinental astenospheric mantle and related mobilization of the slab in our studied area. Furthermore, a large scale process like

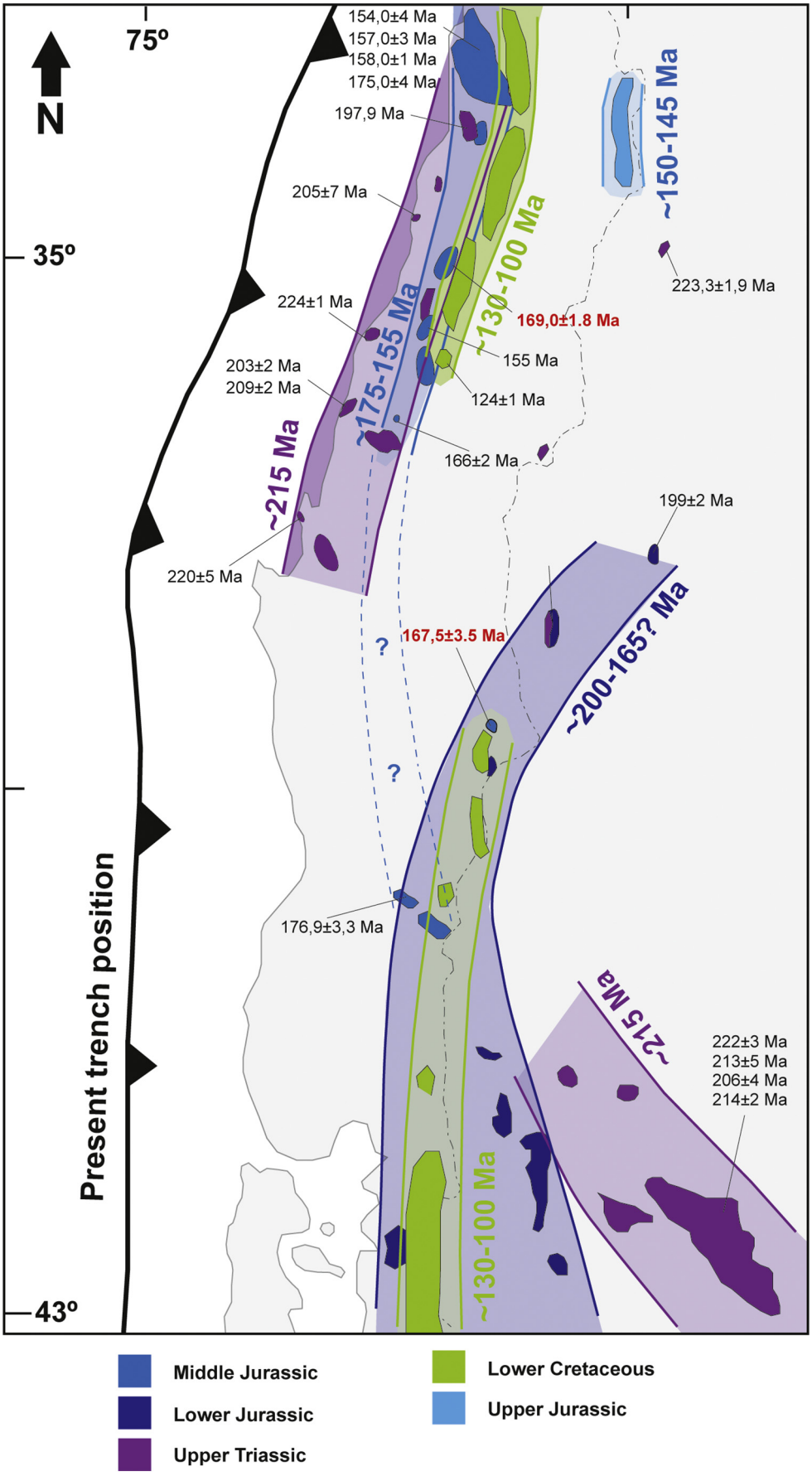

Fig. 9. Proposed variations in arc position during Middle Jurassic to Lower Cretaceous between 33°–35°S.

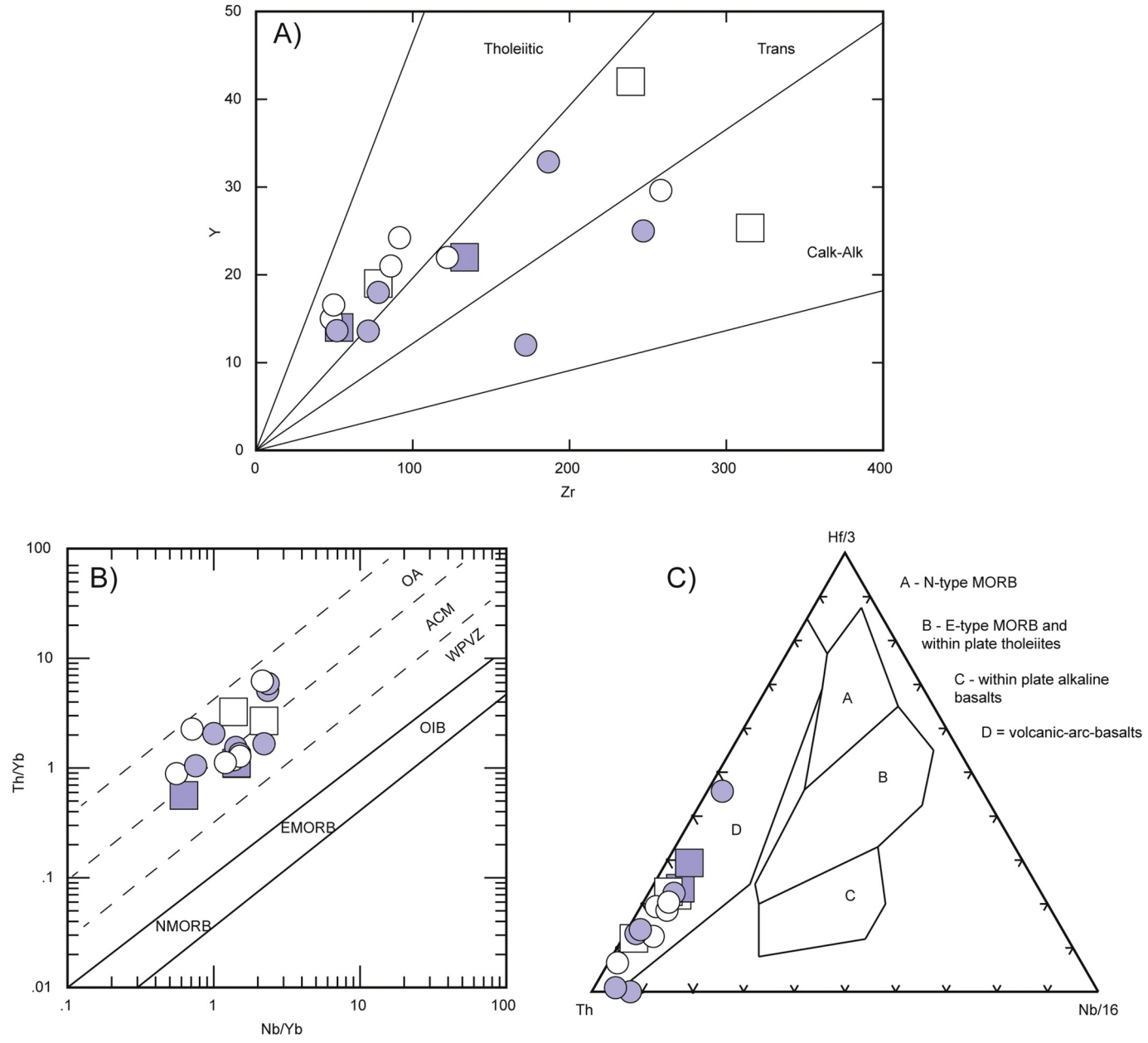

Fig. 10. Discriminant diagrams for the studied rocks. a) Zr versus Y plot according to MacLean and Barrett (1993) showing a dominant tholeiitic to transitional trend for the studied rocks. b) Nb/Yb versus Th/Yb modified after Pearce (1983). The studied samples plot systematically in the subduction related fields. c) Th - Hf/3 - Nb/16 Tectonic setting discrimination diagram (Wood, 1980) for volcanic (basic-intermediate-acid) rocks in the studied area.

slab roll-back should not only influence arc position in the contiguous areas but mantle dynamics and probably the composition of the related magmatism (Magni, 2019). This is consistent with the anomalous enrichment in trace elements and isotopic composition observed in the Middle Jurassic lavas at 33–35°S.

A possible explanation is that slab tearing and roll-back should induce convection of the asthenosphere as a result of the slab drag (Magni, 2019). This dragging should produce a toroidal movement of the mantle removing and exchanging or mixing part of the upper depleted asthenospheric mantle with more fertile, hotter and deeper asthenosphere (Magni, 2019), or as posited by Navarrete et al., (2019), pulling part of the Karoo plume to the west. All these processes seems to explain most of the trace element enrichment observed in the Middle Jurassic magmatism of central Chile, however, not all of them are consistent with some trace elements proxies and isotopic composition of the lavas, giving some constrains for the nature of the genesis of the magmas.

First, melting of the deep mantle lehrzolitic sources should imply low concentrations of HREE. As seen in the presented data, no clear evidences of garnet involvement can be detected, with the exception of slightly higher Sm/Yb ratios in some Altos de Hualmapu Formation samples, so melting, segregation and subsequent fractionation should take place mostly above the garnet lherzolite field. Second, Sr and Nd isotopic data suggest a systematic enrichment for the lavas and almost mimics the values of EMII and BSE (Fig. 6) whereas lead isotopes suggest that samples are over the BSE, in the field of the EMII. The most commonly proposed origin for an EMII reservoir is the recycling of marine pelagic sediments and the upper continental crust. In this context, a possible explanation is that the induced flow from the hotter mantle can trigger a melting of the subducted sediments and/or part of the upper portions of the slab resulting in an isotopic enrichment, especially higher in Pb radiogenic ratios. It is important to note that high degrees of melting of the eclogitized slab could induce the apparition of "adakitic signatures", which is not observed in the values of our samples. In this

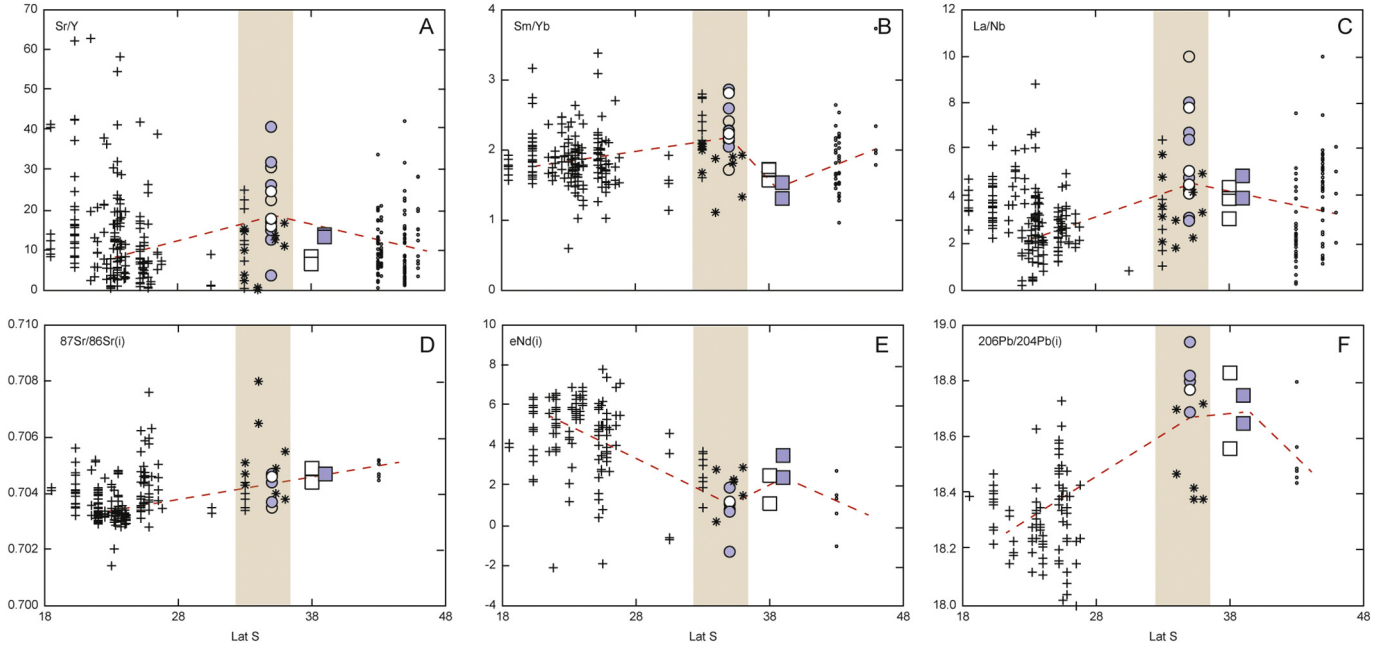

Fig. 11. Sr/Y, Sm/Yb, La/Nb, $^{87}Sr/^{86}Sr_{(i)}$, eNd, and $^{206}Pb/^{204}Pb_{(i)}$ vs location (°) diagrams to evaluate the compositional variations of Jurassic arc magmatism between 18° and 48°S. Highlighted area shows the anomalous enrichment in geochemical proxies in central Chile. Red dashed line marks tendency of mean values at each latitude. References in Supplementary material X.

context, it is more plausible that Pb isotopic signatures reflect the nature of fertile mantle, as presented values overlap those of other intraplate magmatic provinces in Patagonia and the Antarctic Peninsula (Hole, 1990; Stern, 2002).

Other process, such as a local tearing of the slab or break-off in the area cannot be ruled out, since the effects of them in the observed chemistry can explain most of the observed features. In this context, the presence of a small tearing at approximately 37–38°S during the Middle Jurassic can explain discontinuous behavior of the arc front with the volcanism in Lonquimay - Icalma area versus the transition from the Lower Jurassic Cara-Cura and Cordillera del Viento volcanism in actual Argentinian Precordillera, synchronous to the deposition of volcanoclastic sediments of the Rincon de Nuñez Formation in the Coastal Cordillera of Chile to subsequent effusion of Altos de Hualmapuvolcanites in the same area during the Middle Jurassic, coupled to marine deposition to the east. The observed Sr-Nd-Pb isotopic values highly resemble those from other magmatic provinces related to slab windows as Pali-Aike and Antartic peninsula (Hole, 1990; Stern, 2002), suggesting a significative influence of an enriched plume-like mantle.

By comparing some HFSE compositional features of Jurassic Arc magmatism of Southern-Central Chile with other modern and ancient magmatic provinces related to slab tearing or break-off, is possible to conclude, as mentioned before, an origin above the garnet peridotite field, slightly deeper for the Altos de Hualmapu samples, and lower La/Sm values in general, in contrast to typical magmas related to Slab break-off (Fig. 13a). Nb/Ta ratios (Fig. 13b) show values below the chondrite and MORB and in the range of cordilleran batholits. Low Nb/Ta ratios in arc magmas are commonly related to rutile fractionation at high pressures, over 50 km. (Tang et al., 2019), however, Sm/Yb ratios do not suggest garnet as a residual phase in the source, so partial melting of eclogitized subducted slab or arclogites is not possible and this low ratios seems to be an inherit feature of the sub-arc mantle during Jurassic. Finally La/Nb values for studied samples (Fig. 13c) are some of the highest in Jurassic Andean magmatism but in the range of arc

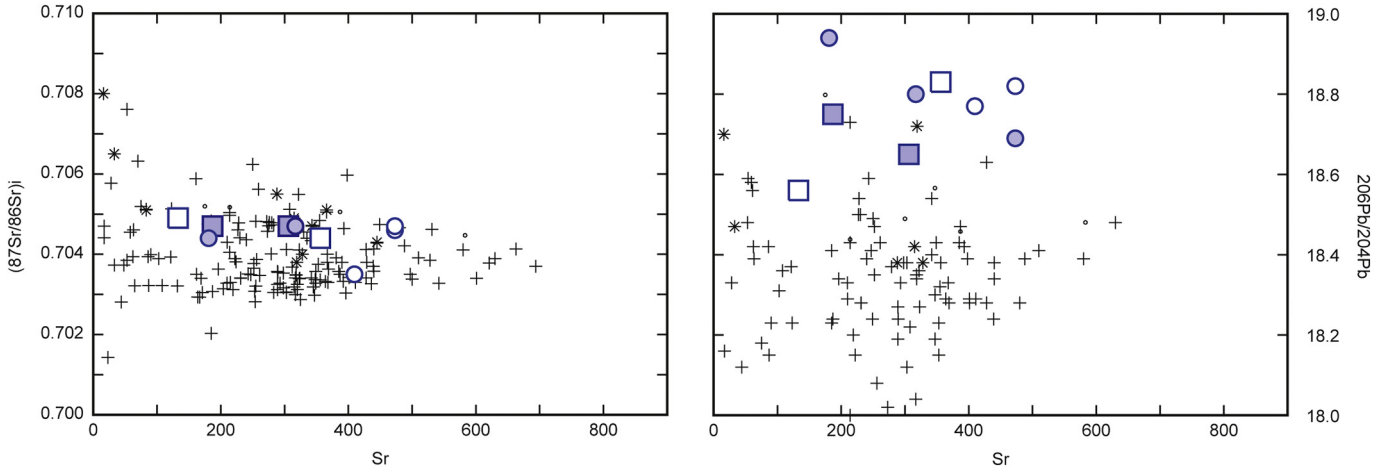

Fig. 12. Map showing the arc position estimation during Early Mezosoic. Modified After Sernageomin, 2003 and Navarrete et al., 2019. Only in-situ igneous U—Pb, Rb—Sr and Ar—Ar geochronology is considered. Data from references in the text and this work (in red).

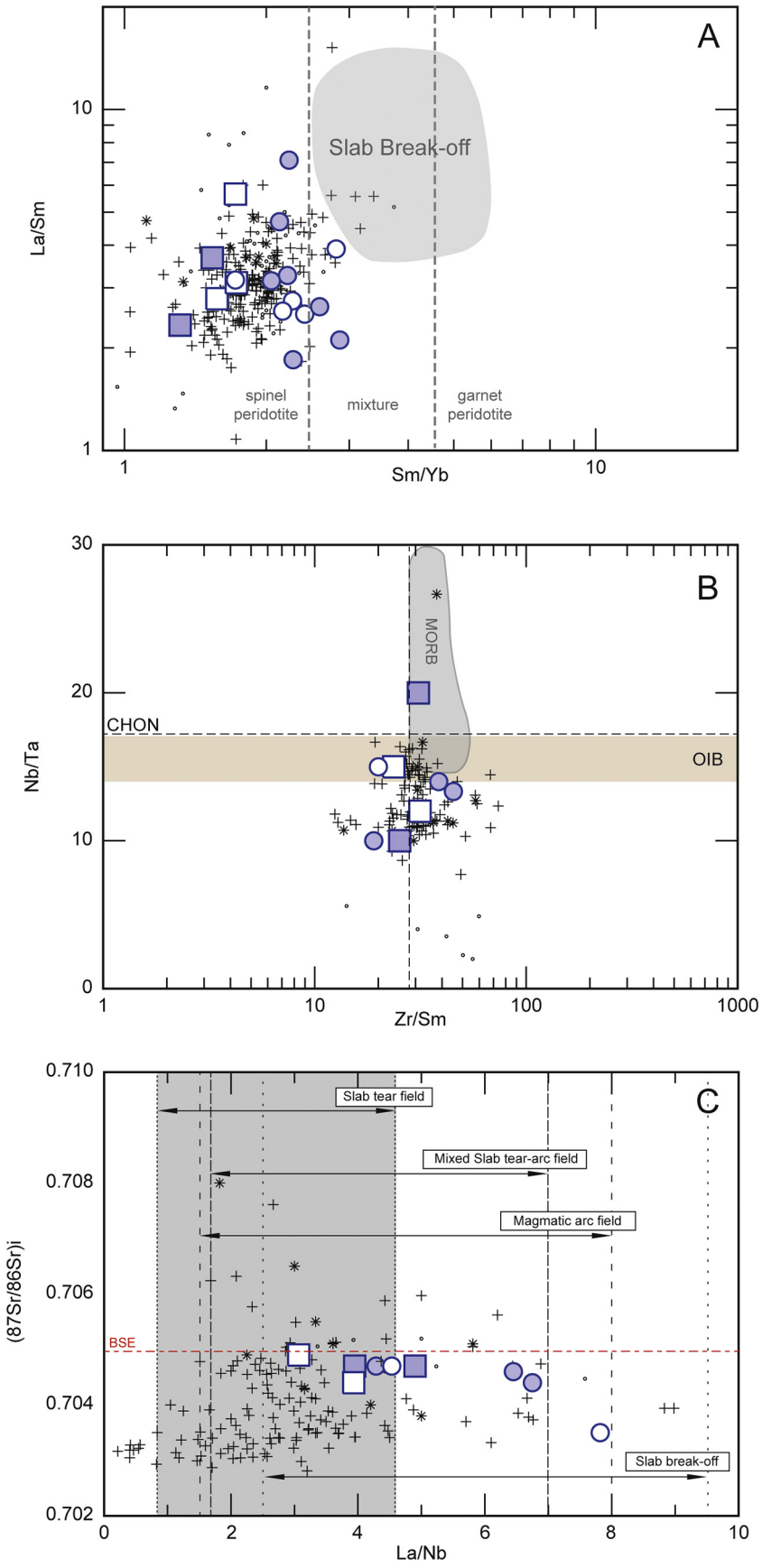

Fig. 13. a) La/Sm vs Sm/Yb, b) Nb/Ta vs Zr/Sm (after Foley et al., 2002) and c) $^{87}Sr/^{86}Sr_{(i)}$ vs La/Nb, (After Rosenbaum et al., 2008) for Jurassic samples from Chile and Argentina.

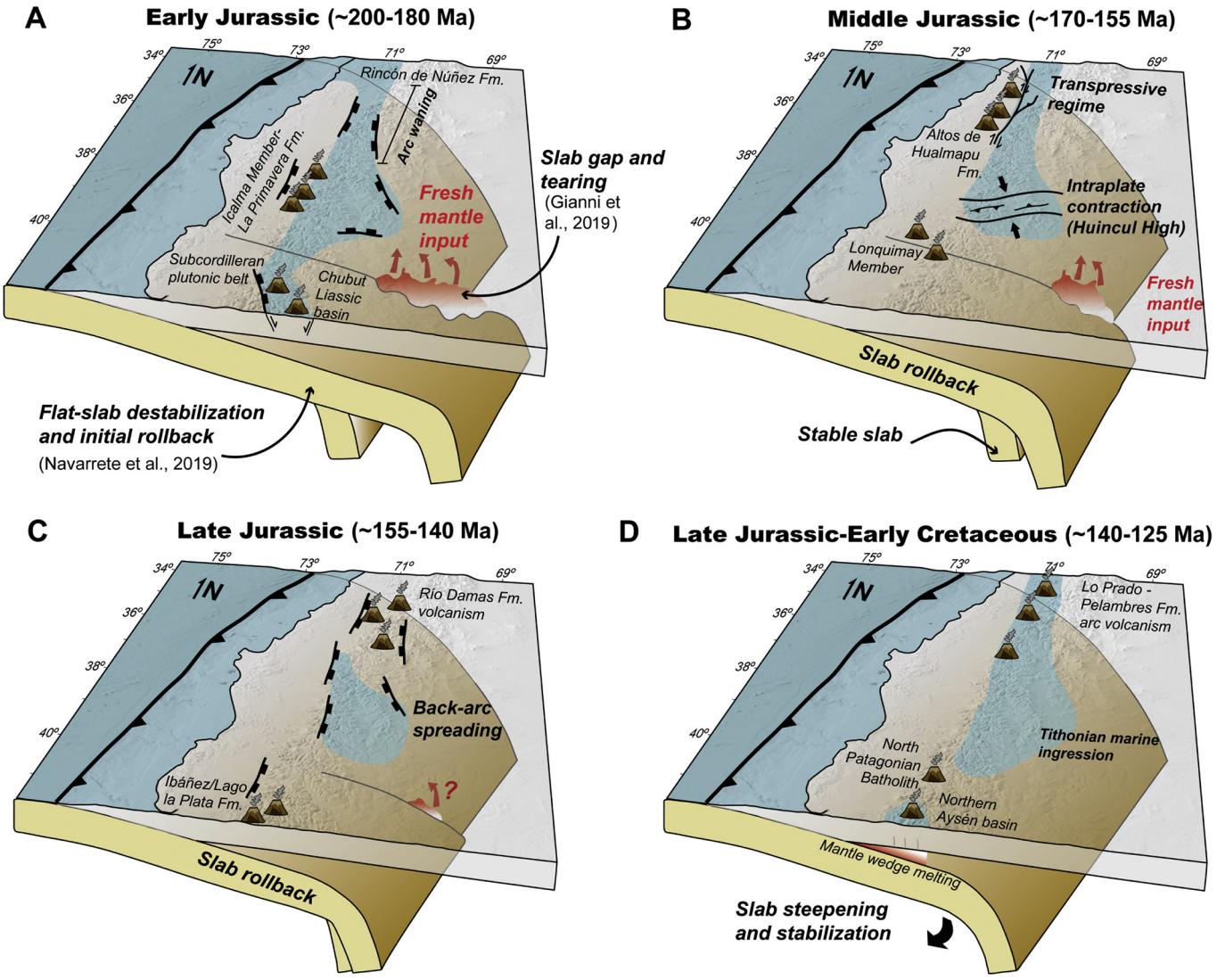

Fig. 14. schematic tectono-magmatic evolution form Lower Jurassic to Lower Cretaceous in Southern Central Chile.

and slab tear field, according to Rosenbaum et al. (2008), which is consistent with the arc related nature of the magmas and the close spatio temporal relation of the studied magmas with the massive slab tearing proposed by Gianni et al. (2019).

In view of the above we propose that the particular compositional features observed in Jurassic Magmatism of Southern-Central Chile are mostly a reflection of the interaction between depleted mantle mixed with small amounts of fertile OIB-like asthenosphere that reach the sub-arc area as result of the large Upper Triassic – Lower Jurassic tearing of the slab at this latitudes (Gianni et al., 2019), which is consistent with previous models that suggest the existence of a "thermal plume" that enhance the production of magmatism during the same period (Llambías et al., 2007).

In view of the chemical and isotopical evidence, coupled with discontinuous distribution of the arc front in the area, is possible to suggest that late Triassic to lower Jurassic tearing of the slab in Patagonia (Gianni et al., 2019) persist at least until Middle Jurassic in the area (36°–38°S), to probably be completely close by Late Jurassic to Lower Cretaceous (Fig. 14).

4. Conclusions

Jurassic magmatism in Southern Central Chile mark the transition between Central and Patagonian segments of Early Andean Magmatic Province (EAMP) and is represented by the middle Jurassic intermediate deposits of the Altos de Hualmapu Formation in Coastal Cordillera (35°S) and the lower basaltic and upper intermediate volcanites of the Nacientes de Biobio Formation in High Andes (39°S). All studied units show typical subduction related affinities (High LILE, over HFSE, positive Pb and negative Nb (Ta) anomalies, etc.) that resemble the characteristics of arcs that transit from younger to mature states but with more enriched characteristics in northern unit. Flat shapes in MREE and HREE suggest segregation and crystallization of the magmas above the garnet lherzolitic field implying a non-thickened crust during this period, which is consistent with the mostly extensional/transtensional conditions during this period. Older evidences of Jurassic arc activity in the area are the ≈200 Ma. lavas an subvolcanic bodies of Cara Cura Formation in western Argentina (36°45′S), basaltic lavas of the lower member of Nacientes del Biobio Formation and an important population of detrital zircons ranging in ages between 188 and 180 Ma. in samples from an epiclastic sandstone from Rincon de Nuñez Formation. No evidence of Jurassic magmatic activity is observed in Coastal Cordillera after 155 Ma. when arc front seems to shift to the east during Upper Jurassic to resume again in actual Coastal Cordillera during Lower Cretaceous, probably as result of slab roll back and back arc extension.

The highly enriched geochemical and isotopic signature of the lavas, respect to northern and Patagonian equivalents, especially in the Altos de Hualmapu Formation, suggest that parental magmas are composed

by a mixture between MORB like magmas (80–70%) and an enriched source (20–30%). Given the mostly extensional to transtensional conditions of the western margin of Gondwana during Jurassic we propose that the most probable source for this enriched endmember should be fertile asthenosphere dragged as result of the massive roll back of the slab in Patagonia and related tearing of the slab under the arc in the area during Upper Triassic and Lower Middle.

Declaration of Competing Interest

The authors declare that they have no known competing financial interests or personal relationships that could have appeared to influence the work reported in this paper.

Acknowledgements

This study was funded through the FONDECYT Iniciación grant 11160329 (Pablo Rossel). Y. Diaz, J. Maturana, P. Zambrano and L. Olivares are thanked for assistance in the field work. B. Godoy and anonymous reviewer are specially thanked for the thorough and detailed corrections and suggestions that significantly improved an earlier version of this manuscript. Mihai N.Ducea acknowledges support from the Romanian Executive Agency for Higher Education, Research, Development and Innovation Funding project, PN-III-P4-ID-PCCF-2016-0014.

Appendix A. Supplementary data

Supplementary data to this article can be found online at https://doi.org/10.1016/j.lithos.2020.105510.

References

Abad, E., Figueroa, J., 2003. Rocas volcánicas en el Triásico del Biobío: Petrografía y marco geológico, cerro Calquinhue, VIII Región; Chile. Congreso Geológico Chileno, No. 10, Actas: 8 p. Concepción.

Aragón, E., Castro, A., Díaz-Alvarado, J., Liu, D.-Y., 2011. The North Patagonian batholith at Paso Puyehue (Argentina–Chile). SHRIMP ages and compositional features. J. S. Am. Earth Sci. 32, 547–554. https://doi.org/10.1016/j.jsames.2011.02.005.

Bechis, F., Cristallini, E., Giambiagi, L., Yagupsky, D., Guzman, C., Garcia, V., 2014. Transtensional tectonics induced by oblique reactivation of previous lithospheric anisotropies during the late Triassic to early Jurassic rifting in the Neuquen basin: Insights from analog models. J. Geodyn. 79, 1–17.

Belmar, M., Morata, D., Munizaga, F., Perez de Arce, C., Morales, S., Carrillo, F.J., 2004. Significance of K-Ar dating of verylow-grade metamorphism in Triassic-Jurassic pelites from the Coastal Range of Central Chile. ClayMinerals 39, 151–162.

Bravo, P., 2001. Geología del Borde Oriental de la Cordillera de la Costa entre los ríos Mataquito y Maule, VII Región. Memoria de Título. (Inédito). Universidad de Chile, Departamento de Geología, Santiago (113 p).

Bruce, Z.R.V., 2001. Mesozoic Geology of the Puerto Ingeniero Ibanez Area, 46° South, Chilean Patagonia. PhD thesis. University of Canterbury.

Buchelt, M., Téllez, C., 1988. The Jurassic La Negra Formation in the area of Antofagasta, northern Chile (lithology, petrography, geochemistry). In: Bahlburg, H., Breitkreuz, C., Giese, P. (Eds.), The Southern Central Andes. Lecture Notes in EarthSciences. 17, pp. 171–182.

Castro, A., Moreno-Ventas, I., et al., 2011. Petrology and SHRIMP U-Pb zircon geochronology of Cordilleran granitoids of the Bariloche area, Argentina. J. S. Am. Earth Sci. 32, 508–530. https://doi.org/10.1016/j.jsames.2011.03.011.

Chapman, J.B., Ducea, M.N., Kapp, P., Gehrels, G.E., DeCelles, P.G., 2017. Spatial and temporal radiogenic isotopic trends of magmatism inCordilleran orogens. Gondwana Res. 48, 189–204.

Charrier, R., Pinto, L., Rodriguez, M.P., 2007. Tectonoestratigraphic evolution of the Andean Orogen in Chile. In: Moreno, T., Gibbons, W. (Eds.), The Geology of Chile. The Geological Society, London, pp. 21–144.

Christensen, N., Mooney, W., 1995. Seismic velocity structure and composition of the continental crust: a global view. J. Geophys. Res. 100, 9761–9788.

Corvalan, J., 1976. El Triasico y Jurasico de Vichuquen-Tilicura y de Hualañe, Provincia de Curico. Implicaciones paleogeograficas. Actas I Congresos Geologico Chileno, pp. A137–A154 t. 1, p.

Craddock, J.P., Schmitz, M.D., Crowley, J.L., Larocque, J., Pankhurst, R.J., Juda, N., Konstantinou, A., Storey, B., 2017. Precise U-Pb zircon ages and geochemistry of Jurassic granites, Ellsworth-Whitmore terrane, Central Antarctica. The Geological Society of America Bulletin 129 (1/2), 118–136. https://doi.org/10.1130/B31485.1.

Creixell, C., Parada, M.A., Morata, D., Vásquez, P., Pérez de Arce, C., Arriagada, C., 2011. Middle-late Jurassic to early cretaceous transtension and transpression during arc building in Central Chile: evidence from mafic dike swarms. Andean Geol. 38 (1), 37–63. https://doi.org/10.5027/andgeoV38n1-a04.

De La Cruz, R., Suárez, M., 1997. El Jurásico de la cuenca de Neuquén en Lonquimay, Chile; Formación Nacientes del BíoBío (38°-39°). Rev. Geol. Chile 24 (1), 3–24 Santiago.

D'Elia, L., Muravchik, M., Franzese, J., Bilmes, A., 2012. Volcanismo de sin-rift de la Cuenca Neuquina, Argentina: relación con la evolución Triásico Tardía-Jurásico Temprano del margen Andino. Andean Geol. 39 (1), 106–132.

Drew, S., Ducea, M., Schoenbohm, L., 2009. Mafic volcanism on the Puna Plateau, NW Argentina: implications for lithospheric composition and evolution with an emphasis on lithospheric foundering. Lithosphere 1, 305–318.

Drosina, M., Barredo, S., Stinco, L., Giambiagi, L., Migliavacca, O., 2017. Petrofísica básica de los depósitos del ciclo Precuyano, Sierra de la Cara Cura, Mendoza. Latin Am. J. Sedimentol. Basin Anal. 24 (2), 75–91.

Ducea, M.N., Saleeby, J.B., 1998. The age and origin of a thick mafic ultramafic root from beneath the Sierra Nevada batholiths. Contrib. Mineral. Petrol. 133, 169–185.

Echaurren, A., Oliveros, V., Folguera, A., Ibarra, F., Creixell, C., Lucassen, F., 2017. Early Andean tectonomagmatic stages in North Patagonia: insights from field and geochemical data. J. Geol. Soc. Lond. 174 (3), 405–422.

Emparan, C., Pineda, G., 2000. Área La Serena-La Higuera, Región de Coquimbo. ServicioNacional de Geología y Minería. Mapas Geológicos 18 Escala 1:100,000. Santiago.

Faure, G., 1986. Principles of Isotope Geology. New York, Chichester, Brisbane, Toronto, 2nd ed. John Wiley & Sons, Singapore xv + 589 pp.

Foley, S., Tiepolo, M., Vannucci, R., 2002. Growth of early continental crust controlled by melting of amphibolite in subduction zones. Nature 417 (6891), 837–840. https://doi.org/10.1038/nature00799.

Gana, P.Y., Tosdal, R.M., 1996. Geocronología U-Pb y K-Ar en intrusivos del Paleozoico y Mesozoico de la Cordillera de la Costa, Región de Valparaíso, Chile. Rev. Geol. Chile 23 (2), 151–164.

Gianni, G.M., Navarrete, C., Spagnotto, S., 2019. Surface and mantle records reveal an ancient slab tear beneath Gondwana. Sci. Rep. 9, 19774. https://doi.org/10.1038/s41598-019-56335-9.

Gordon, A., Ort, M., 1993. Edad y correlación del plutonismo subcordillerano en las provincias de Río Negro y Chubut. XII Congreso Geológico Argentino actas 4: 120-127. Mendoza.

Grocott, J., Taylor, G.K., 2002. Magmatic arc fault systems, deformation partitioning and emplacement of granitic complexes in the Coastal Cordillera, north Chilean Andes (25°30′S to 27°00′S). J. Geol. Soc. Lond. 159 (4), 425–442.

Grove, T.L., Parman, S.W., Bowring, S.A., Price, R.C., Baker, M.B., 2002. The role of H2O-rich fluids in the generation of primitive basaltic andesites and andesites from Mt. Shasta region, N. California. Contribution to Mineralogy and Metrology. vol 142, pp. 375–396.

Hart, S.R., 1984. A large-scale isotope anomaly in the Southern Hemisphere mantle. Nature 309, 753–757.

Hervé, F., Pankhurst, R.J., Fanning, C.M., Calderón, M., Yaxley, G.M., 2007. The south Patagonian batholith: 150 my of granite magmatism on a plate margin. Lithos 97, 373–394. https://doi.org/10.1016/j.lithos.2007.01.007.

Hole, M.J., 1990. Geochemical evolution of Pliocene – recent post subduction alkaline basalts from seal nunataks, Antartic Peninsula. J. Volcanol. Geotherm. Res. 40, 149–167.

Junkin, W.D., Gans, P.B., 2019. Stratigraphy and geochronology of the Nacientes del Teno and Río Damas Formations: insights into Mid-dle to Late Jurassic Andean volcanism. Geosphere 15 (2), 450–478. https://doi.org/10.1130/GES01698.1.

Kramer, W., Siebel, W., Romer, R., Haase, G., Zimmer, M., Ehrlichmann, R., 2005. Geochemical and isotopic characteristics and evolution of the Jurassic volcanic arc between Arica (18°30′S) and Tocopilla (22°S), North Chilean Coastal Cordillera. Chem. Erde 65, 47–78.

Lamb, S., Davis, P., 2003. Cenozoic climate change as a possible cause for the rise of the Andes. Nature 425 (6960), 792–797. https://doi.org/10.1038/nature02049.

LeMaitre, R.W., 1989. A Classification of Igneus Rocks and Glossary of Therms. Blackwell Scientific Publication, London (193 pp.).

Llambías, E.J., Leanza, H.A., Carbone, O., 2007. Evolución tectono-magmática durante el Pérmico al Jurásico Temprano en la cordillera del Viento (37°05′S - 37°15′S): nuevas evidencias geológicas y geoquímicas del inicio de la cuenca Neuquina. Rev. Asoc. Geol. Argent. 62 (2), 217–235.

Lucassen, F., Kramer, W., Bartsch, V., Wilke, H.G., Franz, G., Romer, R.L., Dulski, P., 2006. Nd, Pb and Sr isotope composition of juvenilemagmatismintheMesozoiclargemagmatic province of northern Chile (18°–27°S): indications for a uniform subarc mantle. Contrib. Mineral. Petrol. 152, 571–589.

MacLean, W.H., Barrett, T.J., 1993. Lithogeochemical techniques using immobile elements. J. Geochem. Explor. 48, 109–133.

Magni, V., 2019. The effects of back-arc spreading on arc magmatism. Earth Planet. Sci. Lett. 519, 141–151.

Mantle, G.W., Collins, W.J., 2008. Quantifying crustal thickness variations in evolving orogens: correlation between arc basalt composition and Moho depth. Geology 36, 87–90. https://doi.org/10.1130/g24095a.1.

Mazzini, A., Svensen, H., Leanza, H.A., Corfu, F., Planke, S., 2010. Early Jurassic shale chemostratigraphy and U-Pb ages from the Neuquén Basin (Argentina): implications for the Toarcian Oceanic anoxic event. Earth Planet. Sci. Lett. 297, 633e645.

Mescua, J.F., Giambiagi, L.B., Bechis, F., 2008. Evidencias de tectónica extensional en el Jurásico tardío (Kimeridgiano) del suroeste de la provincia de Mendoza. Rev. Asoc. Geol. Argent. 63 (4), 512–519.

Morel, R., 1981. Geologia del sector norte de la hoja Gualleco, entre los 35°00′ y los 35°10′ latitud sur, provincia de Talca, VII Region, Chile. Tesis de Grado, MCs.Universidad de Chile, Departamento de Geología, Santiago

Mpodozis, C., Kay, S., 1990. Provincias magmaticas acidas y evoluciontectonica de Gondwana: Andes chilenos (28-31°S). Andean Geol. 17 (2), 153–180.

Mpodozis, C., Kay, S., 1992. Late Paleozoic to Triassic evolution of the Gondwana margin: evidence from Chilean Frontal Cordilleran batholiths (28 to 31°S). Geol. Soc. Am. Bull. 104, 999–1014.

Mpodozis, C., Ramos, V., 1989. The Andes of Chile and Argentina. In: Ericksen, G.E., Cañas, M.T., Reinemund, J.A. (Eds.), Geology of the Andes and its Relation to Hydrocarbon and Energy Resources. Circum Pacific Council for Energy and Hydrotermal Resources, Huston, Earth Science Series. 11, pp. 59–90.

Naipauer, M., García Morabito, E., Marques, J.C., Tunik, V., Rojas Vera, E., Vujovich, G.I., Pimentel, M.P., Ramos, V.A., 2012. Intraplate late Jurassic deformation and exhumation in western Central Argentina: constraints from surface data and U-Pb detrital zircon ages. Tectonophysics 524e525 (1), 59e75.

Naipauer, M., Tunik, M., Marques, J.C., Rojas-Vera, E., Vujovich, G.I., Pimentel, M.M., Ramos, V.A., 2015. U-Pb detrital zircon ages of Upper Jurassic continental successions: Implications for the provenance and absolute age of the Jurassic-cretaceous boundary in the Neuquén Basin. GeolSoc. 399(1). Special Publications, London, pp. 131–154.

Navarrete, C., Gianni, G., Echaurren, A., LinceKingler, F., Folguera, A., 2016. Episodic Jurassic to lower cretaceous intraplate compression in Central Patagonia during Gondwana breakup. J. Geodyn. 102, 185–201.

Navarrete, C., Gianni, G., Encinas, A., Marquez, M., Kemerbeek, Y., Valle, M., Folguera, A., 2019. Triassic to Middle Jurassic geodynamic evolution of southwestern Gondwana: from large flat-slab to mantle plume suction in a rollback subduction setting. Earth Sci. Rev. 194, 125–159.

Oliveros, V., Vasquez, P., Creixell, C., Lucassen, F., Ducea, M.N., Ciocca, I., Gonzalez, J., Espinoza, M., Salazar, E., Coloma, F., Kaseman, S., 2019. Lithospheric evolution of the Pre- and early Andean convergent margin, Chile. Gondwana Res. 80, 202–227.

Pankhurst, R.J., Leat, P.T., Sruoga, P., Rapela, C.W., Márquez, M., Storey, B.C., Riley, T.R., 1998. The Chon Aike province of Patagonia and related rocks in West Antarctica: a silicic large igneous province. J. Volcanol. Geotherm. Res. 81, 113–136. https://doi.org/10.1016/S0377-0273(97) 00070-X.

Pankhurst, R.J., Weaver, S.D., Hervé, F., Larrondo, P., 1999. Mesozoic–Cenozoic evolution of the North Patagonian Batholith in Aysén, southern Chile. J. Geol. Soc. Lond. 156, 673–694. https://doi.org/10.1144/gsjgs.156.4.0673.

Pankhurst, R.J., Hervé, F., Fanning, M., Suárez, M., 2003. Coeval plutonic and volcanic activity in the Patagonian Andes: The Patagonian Batholith and the Ibáñez and Divisadero formations, Aysén, Southern Chile. Congreso Geológico Chileno, Concepción, CD-ROM.

Paterson, S.R., Ducea, M.N., 2015. Arc Magmatic Tempos: gathering the evidence. Elements 11 (2), 91–97.

Pearce, J.A., 1983. Role of the sub-continental lithosphere in magma genesis at active continental margins. In: Hawkesworth, C.J., Norry, M.J. (Eds.), Continental Basalts and Mantle Xenoliths. Shiva, Nentwich, pp. 230–249.

Pearce, J.A., Wyman, D.A., 1996. A users guide to basalt discrimination diagrams. Trace Element Geochemistry of Volcanic Rocks: Applications for Massive Sulphide Exploration. Geological Association of Canada, pp. 79–113 Short Course Notes12.

Pesicek, J.D., Engdahl, E.R., Thurber, C.H., DeShon, H.R., Lange, D., 2012. Mantle subducting slab structure in the region of the 2010 *M*8.8 Maule earthquake (30–40°S), Chile. Geophys. J. Int. 191 (1), 317–324.

Ramírez Arellano, C., Putlitz, B., Müntener, O., Ovtcharova, M., 2012. High precision U/Pb zircon dating of the Chaltén Plutonic complex (Cerro Fitz Roy, Patagonia) and its relationship to arc migration in the southernmost Andes. Tectonics 31 (4).

Rapela, C.W., Dias, C.F., Francese, J.R., Alonso, G., Benvenuto, A.R., 1991. Elbatolito de la Patagonia central: evidencias de un magmatismo triásico-jurásicoasociado a fallas transcurrentes. Rev. Geol. Chile 18, 121–138.

Rapela, C.W., Pankhurst, R.J., Fanning, C.M., Hervé, F., 2005. Pacific subduction coeval with the Karoo mantle plume: the Early JurassicSubcordilleran belt of northwestern Patagonia. In: Vaughan, A.P.M., Leat, P.T., Pankhurst, R.J. (Eds.), Terrane Processes at the Margins of Gondwana. Geological Society. 246. Special Publications, London, pp. 217–239. https://doi.org/10.1144/GSL.SP.2005.246.01.07.

Riley, Teal R., Flowerdew, Michael J., Pankhurst, Robert J., Curtis, Mike L., Millar, Ian L., Mark Fanning, C., Whitehouse, Martin J., 2016. Early Jurassic magmatism on the Antarctic Peninsula and potential correlation with the Subcordilleran plutonic belt of Patagonia. J. Geol. Soc. 174, 365–376. https://doi.org/10.1144/jgs2016-053 3 November.

Ring, U., Willner, A., Layer, P., Richter, P., 2012. Jurassic to early cretaceous postaccretionalsinistraltranspression in northcentral Chile (latitudes 31-32°S). Geol. Mag. 149 (2), 202–220.

Rossel, P., Oliveros, V., Ducea, M., Charrier, R., Scaillet, S., Retama, L., Figueroa, O., 2013. The early Andean Subduction System as an analogue to island arcs: evidence from across-arc geochemical variations in northern Chile. Lithos 179 (2), 211–230.

Rossel, P., Oliveros, V., Mescua, J., Tapia, F., Ducea, M.N., Calderon, S., Charrier, R., Hoffman, D., 2014. The Upper Jurassic volcanism of the Río Damas-Tordillo Formation (33°-35.5°S): Insights on petrogenesis, chronology, provenance and tectonic implications. Andean Geol. 41 (3), 529–557.

Rosenbaum, G., Gasparon, M., Lucente, F.P., Peccerillo, A., Miller, M.S., 2008. Kinematics of slab tear faults during subduction segmentation and implications for Italian magmatism. Tectonics 27.

SEGEMAR, 1995. Geologic Map of Argentina digital version, 1:2500000.

Scheuber, E., González, G., 1999. Tectonics of the Jurassic–early cretaceous magmatic arc of the north Chilean Coastal Cordillera (22°–26°S): a story of crustal deformation along a convergent plate boundary. Tectonics 18, 895–910.

Scholl, D., von Huene, R., 2010. Subduction zone recycling processes and the rock record of crustal suture zones. Can. J. Earth Sci. 47 (5), 633–654.

Sernageomin, 2003. Mapa Geológico de Chile: versión digital. Servicio Nacional deGeología y Minería. 4. PublicaciónGeológica Digital, Santiago.

Stern, R.J., 2002. Subduction zones. Rev. Geophys. 40, 1031–1039. https://doi.org/10.1029/2001RG000108.

Suárez, M., Demant, A., De la Cruz, R., 1999. Volcanismo calco-alcalino en W Provincia Chon Aike: Grupo Ibáñez, Jurásico Superior–Cretácico Inferior temprano, Cordillera Patagónica de Aysén, Chile (45°30′–46°30'S). In: Salfity, J.A., et al. (Eds.), Congreso Geológico Argentino. Salta, Actas II, pp. 186–189.

Suárez, M., De la Cruz, R., Aguirre-Urreta, B., Fanning, M., 2009. Relationship between volcanism and marine sedimentation in northern Austral (Aisén) Basin, Central Patagonia: Stratigraphic, U–Pb SHRIMP and paleontologic evidence. J. S. Am. Earth Sci. 27, 309–325.

Sun, S.S., McDonough, W.F., 1989. Chemical and isotopic systematics of oceanic basalts: implications for mantle composition and processes. Geol. Soc. Spec. Publ. 42, 313–345.

Tang, M., Lee, C.A., Chen, K., et al., 2019. Nb/Ta systematics in arc magma differentiation and the role of arclogites in continent formation. Nat Commun 10, 235. https://doi.org/10.1038/s41467-018-08198-3.

Tunik, M., Folguera, A., Naipauer, M., Pimentel, M., Ramos, V.A., 2010. Early uplift and orogenic deformation in the Neuquen basin: Constraints on the Andean uplift from U-Pb and Hf isotopic data of detrital zircons. Tectonophysics 489, 258–273.

Vásquez, P., Glodny, J., Franz, G., Frei, D., Romer, R.L., 2011. Early Mesozoic Plutonism of the Cordillera de la Costa (34°–37°S), Chile: constraints on the onset of the Andean Orogeny. J. Geol. 119 (2), 159–184.

Vergara, M., Levi, B., Nystrom, J., Cancino, A., 1995. Jurassic and early cretaceous island arc volcanism, extension, and subsidence in the Coast Range of Central Chile. Geol. Soc. Am. Bull. 107, 1427–1440.

Wall, R., Gana, P., Gutierrez, A., 1996. Mapa Geológico del área San Antonio-Melipilla, Regiones de Valparaíso, Metropolitana y del Libertador General Bernardo O'Higgins. Servicio Nacional de Geología y Minería, Mapas Geológicos N° 2 escala 1:100.000.

Wasserburg, G.J., Jacobsen, S.B., DePaolo, D.J., McCulloch, M.T., Wen, T., 1981. Precise determination of Sm/Nd ratios, Sm and Nd isotopic abundances in standard solutions. GeochimicaetCosmochimicaActa 45, 2311–2323.

Willner, A.P., 2005. Pressure Temperature evolution of a late Paleozoic paired metamorphic belt in North-Central Chile (34°–35°30'S). J. Petrol. 46 (9), 1805–1833.

Wood, D.A., 1980. The application of a Th-Hf-Ta diagram to problems of tectonomagmaticcassification and to establishing the nature of Cristal contamination of basaltic lavas of the British Tertiary Volcanic Province. Earth Planet. Sci. Lett. 50, 11–30.

Zaffarana, C., Somoza, R., Lopez de Luchi, M., 2014. The late Triassic Central Patagonian Batholith: Magma hybridization, $^{40}Ar/^{39}Ar$ ages and thermobarometry. J. S. Am. Earth Sci. 55, 94–122.